Lymphocryptovirus Infection of Nonhuman Primate B Cells Converts Destructive into Productive Processing of the Pathogenic CD8 T Cell Epitope in Myelin Oligodendrocyte Glycoprotein.

Jagessar, S.A.; Holtman, I.R.; Hofman, S.; Morandi, E.; Heijmans, N.; Laman, J.D.; ... ; 't, Hart B.A.

Lymphocryptovirus Infection of Nonhuman Primate B Cells Converts Destructive into Productive Processing of the Pathogenic CD8 T Cell Epitope in Myelin Oligodendrocyte Glycoprotein

S. Anwar Jagessar, Inge R. Holtman, Sam Hofman, Elena Morandi, Nicole Heijmans, Jon D. Laman, Bruno Gran, Bart W. Faber, Sander I. van Kasteren, Bart J. L. Eggen and Bert A. 't Hart

J Immunol published online 13 July 2016
http://www.jimmunol.org/content/early/2016/07/13/jimmunol.1600124

The Journal of Immunology is published twice each month by The American Association of Immunologists, Inc., 9650 Rockville Pike, Bethesda, MD 20814-3994.

Print ISSN: 0022-1767 Online ISSN: 1550-6606.

Published July 13, 2016, doi:10.4049/jimmunol.1600124

Lymphocryptovirus Infection of Nonhuman Primate B Cells Converts Destructive into Productive Processing of the Pathogenic CD8 T Cell Epitope in Myelin Oligodendrocyte Glycoprotein

S. Anwar Jagessar,*,†,‡ Inge R. Holtman,§ Sam Hofman,* Elena Morandi,¶ Nicole Heijmans,* Jon D. Laman,§ Bruno Gran,¶ Bart W. Faber,‖ Sander I. van Kasteren,# Bart J. L. Eggen,§ and Bert A. 't Hart*,†,§

EBV is the major infectious environmental risk factor for multiple sclerosis (MS), but the underlying mechanisms remain obscure. Patient studies do not allow manipulation in vivo. We used the experimental autoimmune encephalomyelitis (EAE) models in the common marmoset and rhesus monkey to model the association of EBV and MS. We report that B cells infected with EBV-related lymphocryptovirus (LCV) are requisite APCs for MHC-E–restricted autoaggressive effector memory CTLs specific for the immunodominant epitope 40-48 of myelin oligodendrocyte glycoprotein (MOG). These T cells drive the EAE pathogenesis to irreversible neurologic deficit. The aim of this study was to determine why LCV infection is important for this pathogenic role of B cells. Transcriptome comparison of LCV-infected B cells and CD20$^+$ spleen cells from rhesus monkeys shows increased expression of genes encoding elements of the Ag cross-presentation machinery (i.e., of proteasome maturation protein and immunoproteasome subunits) and enhanced expression of MHC-E and of costimulatory molecules (CD70 and CD80, but not CD86). It was also shown that altered expression of endolysosomal proteases (cathepsins) mitigates the fast endolysosomal degradation of the MOG40–48 core epitope. Finally, LCV infection also induced expression of LC3-II$^+$ cytosolic structures resembling autophagosomes, which seem to form an intracellular compartment where the MOG40–48 epitope is protected against proteolytic degradation by the endolysosomal serine protease cathepsin G. In conclusion, LCV infection induces a variety of changes in B cells that underlies the conversion of destructive processing of the immunodominant MOG40–48 epitope into productive processing and cross-presentation to strongly autoaggressive CTLs. ***The Journal of Immunology*****, 2016, 197: 000–000.**

Experimental autoimmune encephalomyelitis (EAE) is the best characterized animal model of the human autoimmune neurologic disease multiple sclerosis (MS) (1, 2). Mouse and rat EAE models are frequently used for translational research into the immunopathogenesis of MS and for the development of successful immune-modulatory/-suppressive treatments, with which the progressive loss of neurologic functions can be slowed down.

T cells have a core pathogenic role in the EAE model, but it is unclear whether data obtained in inbred/specific pathogen–free rodents can be directly translated to the pathogen-educated immune system of outbred primates (3). In recent years, we investigated the distinct pathogenic roles of autoaggressive CD4$^+$ and CD8$^+$ T cells in nonhuman primate models of MS: EAE in the small-bodied common marmoset (*Callithrix jacchus*) and the larger-bodied rhesus macaque (*Macaca mulatta*). The similarities of these models with rodent EAE models on the one hand and with MS on the other hand determine their validity for translational research into the immunopathogenesis of MS (4).

We reported that full clinical evolution of EAE in marmosets involves two pathogenic pathways. Similar to mouse EAE models, the pathway that initiates EAE involves the activation of MHC class II–restricted CD4$^+$ Th1 and/or Th17 cells. At a later disease stage, a second pathway is activated that drives EAE progression to irreversible

*Department of Immunobiology, Biomedical Primate Research Centre, 2288GJ Rijswijk, the Netherlands; †Department of Immunology, Erasmus University Medical Center, 3015CE Rotterdam, the Netherlands; ‡MS Centre ErasMS, 3015CE Rotterdam, the Netherlands; §Department of Neuroscience, University Medical Center, University Groningen, 9713AV Groningen, the Netherlands; ¶Division of Clinical Neuroscience, University of Nottingham School of Medicine, NG7 2UH Nottingham, United Kingdom; ‖Department of Parasitology, Biomedical Primate Research Centre, 2288GJ Rijswijk, the Netherlands; and #Leiden Institute of Chemistry and The Institute for Chemical Immunology, Leiden University, 2333CC Leiden, the Netherlands

ORCIDs: 0000-0002-4183-9588 (S.A.J.); 0000-0001-9752-4756 (I.R.H.); 0000-0002-0174-1375 (S.H.); 0000-0002-8222-1514 (E.M.); 0000-0001-5085-9807 (J.D.L.); 0000-0001-6384-2342 (B.G.); 0000-0001-6808-1204 (B.W.F.); 0000-0003-3733-818X (S.I.v.K.).

Received for publication January 20, 2016. Accepted for publication June 6, 2016.

This work was supported by Dutch Multiple Sclerosis Research Foundation Grant 12-777 MS and by an internal grant from the Biomedical Primate Research Centre.

Address correspondence and reprint requests to Prof. Bert A. 't Hart, Department of Immunobiology, Biomedical Primate Research Centre, P.O. Box 3306, 2288GJ Rijswijk, the Netherlands. E-mail address: hart@bprc.nl

The online version of this article contains supplemental material.

Abbreviations used in this article: BLC, B lymphoblastoid cell; BPRC, Biomedical Primate Research Centre; CatC, cathepsin C; CatD, cathepsin D; CatG, cathepsin G; CatH, cathepsin H; Cj-BLC, marmoset BLC; Cj-MOG, MOG sequence of marmoset; Cj-PBMC, marmoset PBMC; Cj-SC, marmoset SC; CMK, Z-glycyl-leucyl-phenylchloromethyl ketone; DC, dendritic cell; EAE, experimental autoimmune encephalomyelitis; EBV–B95-8, EBV-producing cell line B95-8; HV papio, herpes papio virus strain S594; LC3, L chain 3; LCV, lymphocryptovirus; LIR, LC3-interacting region; Mm-BLC, rhesus monkey BLC; Mm-MOG, MOG sequence of rhesus monkey; Mm-PBMC, rhesus monkey PBMC; Mm-SC, rhesus monkey SC; MNC, mononuclear cell; MOG, myelin oligodendrocyte glycoprotein; MS, multiple sclerosis; PAD, peptidyl arginase deaminase; PCA, principal component analysis; qPCR, quantitative PCR; rhMOG, recombinant human MOG; SC, spleen cell; UMCG, University Medical Center Groningen.

neurologic deficits. The latter pathway involves MHC class I/Caja-E–restricted $CD8^+CD56^+$ autoaggressive CTLs specific for myelin oligodendrocyte glycoprotein (MOG). A similar subset of HLA-E–restricted CTLs was identified recently in MS lesions (5), albeit with specificity for myelin basic protein.

In marmoset EAE, T cell autoimmunity against MOG is indispensable for the induction of chronic inflammation (6). The two immunodominant T cell epitopes are localized in the extracellular domain: residues 24–36, which activate Caja-DRB*W1201–restricted $CD4^+$ Th1 cells, and residues 40–48, which activate Caja-E–restricted autoaggressive $CD8^+CD56^+$ CTLs (7–9). Intriguingly, when marmosets were immunized with recombinant human MOG (rhMOG), representing the full-length extracellular domain (1–125), formulated with IFA, we observed only T cell activation against the MOG24–36 epitope (10). However, in marmosets immunized with synthetic MOG34–56 in IFA, we observed activation of CTLs recognizing the MOG40–48 epitope associated with full-blown clinical EAE (11). These observations led us to hypothesize that the strongly pathogenic MOG40–48 epitope is destroyed during processing.

In our search for an APC type that has the capacity to cross-present the exogenous MOG epitope via Caja-E to the autoaggressive CTLs, we found evidence for a crucial pathogenic role for B cells naturally infected with the EBV-related lymphocryptovirus (LCV) CalHV3 (12). We observed that the opposite clinical effect in relapsing-remitting MS of an anti-CD20 Ab (ofatumumab) and atacicept, a soluble antagonist of the B cell cytokines BAFF and APRIL (not effective), could be replicated in marmoset EAE (13, 14). The paradoxical clinical effects could be correlated with differential depletion of CalHV3-infected B cells (15).

In the current study, we investigated Ag presentation by LCV-infected B lymphoblastoid cells (BLCs) in the marmoset and rhesus monkey EAE models. B cells are professional APCs capable of in vivo capture and internalization of low-dose exogenous Ags via their BCR to process the endocytosed Ag in the endolysosomal compartment and to present peptides via constitutively expressed MHC class II molecules to $CD4^+$ T cells in conjunction with costimulatory molecules (CD40, CD80/86) (16). However, presentation of exogenous antigenic peptides via MHC class I to $CD8^+$ T cells in vivo is thought to be essentially confined to dendritic cells (DCs) (17). Under nonpathogenic conditions, B cells cannot exert this function in vivo. However, we (15, 18) found that infusion of autologous LCV-infected B cells, prepulsed in vitro with MOG34–56, into healthy rhesus monkeys or marmosets elicited $CD8^+$ T cell activation in vivo. Therefore, the hypothesis tested in the current study is that LCV infection of B cells leads to limited processing of the exogenous encephalitogenic peptide MOG34–56 in such a way that the MOG40–48 epitope remains available for loading on MHC-E molecules and presentation to core pathogenic $CD8^+$ T cells in the primate EAE model.

We searched for parallels with a cell type of undisputed cross-presentation capacity: the $CD8\alpha^+$ mouse DC. The superior capacity of this DC subset to present exogenous Ag via MHC class I to $CD8^+$ T cells is due to activation of the Ag cross-presentation machinery and impediment of fast Ag degradation by storage in protease-poor prelysosomal endosomes (19). Concerning the first issue, we report a parallel transcriptome analysis of primary and LCV-infected B cells showing that the virus induces multiple changes associated with Ag cross-presentation, including increased expression of MHC class Ib and costimulatory molecules, assembly of immunoproteasome, and modulation of endolysosomal protease-expression profiles. Regarding the second issue, we report that, during the processing in primary B cells, the MOG40–48 epitope is destroyed by the endolysosomal protease cathepsin G (CatG). Of special interest concerning the second issue is the observation that LCV infection induces expression of the autophagosome marker L chain 3 (LC3)-II, suggesting activation of the autophagy pathway, which was implicated in Ag cross-presentation (20). We report that the CTL epitope MOG40–48 contains an LC3-interacting region (LIR) motif (21), ^{44}FSRV^{47}, which is destroyed through cleavage at the Arg^{46} residue by CatG. We found that substitution of the Arg^{46} residue by Cit, a modification potentially occurring in LCV-infected B cells via upregulation of peptidyl arginine deaminase (PAD)2 and PAD4, protects the 35–51 epitope, as well as the MOG40–48 epitope embedded therein, against degradation.

In summary, we propose that LCV infection of B cells converts destructive processing of MOG, which is a tolerogenic mechanism (22), into productive processing enabling cross-presentation of the pathogenic MOG40–48 epitope to autoaggressive CTLs. We propose this paradigm as a mechanistic explanation contributing to the well-established, but poorly understood, association between EBV and MS.

Materials and Methods

Animals and cells

Mononuclear cells (MNCs) were isolated from venous blood (PBMCs) and spleen cells (SCs) from rhesus monkeys (*M. mulatta*) and common marmosets (*C. jacchus*). The monkeys originated from the purpose-bred colonies at the Biomedical Primate Research Centre (BPRC). Blood was collected from sedated animals by venipuncture (femoral vein) and collected into heparinized vacutainers. Spleens were collected at necropsy of animals that were sacrificed for reasons not related to this study and immediately processed for isolation of MNCs. All procedures were reviewed and approved by the Experimental Animal Care and Use Committee of the BPRC.

Blood MNCs from marmosets were infected with supernatant from the EBV-producing cell line B95-8 (EBV–B95-8), and blood MNCs from rhesus monkeys were infected with supernatant of the herpes papio virus strain S594 (HV papio) (23). B lymphoblastoid cell lines (BLCs) were generated as previously described (15, 18).

Isolation of MNC fractions and preparation of lysates

MNCs were prepared from blood and spleen as described (12, 24). $CD20^+$ B cells were isolated using MicroBeads (Miltenyi Biotec, Leiden, the Netherlands), according to the manufacturer's instructions. The residual $CD20^-$ cell fraction was used as a source of myeloid APCs.

For preparation of cell-free lysates, pelleted SCs (20–50 million) were frozen at −80°C and subsequently dissolved in 120 μl of 50 mM citrate buffer + 5 mM DTT + 0.1% Triton X-100 (pH 5). Subsequently, cells were sonicated twice (settings in W) for 30 s with 30-s intervals while cooling on ice, using a Braun sonicator with a 5-mm tip (Braun), to obtain cell-free lysates. Thereafter, lysates were centrifuged in an Eppendorf centrifuge, at 13,200 rpm, for 20 min at 4°C. Supernatants were collected, and protein concentrations were determined by NanoDrop (ThermoFisher Scientific, Wilmington, DE).

RNA sequencing of primary and LCV-infected B cells from rhesus monkeys

RNA was isolated from unfractionated rhesus monkey SCs (Mm-SC), SCs separated into $CD20^+$ or $CD20^-$ using an anti-human CD20 mAb and magnetic bead separation (indicated as $CD20^+$ and $CD20^-$ SC), and rhesus monkey BLCs (Mm-BLCs). Illumina HiSEquation 2000S single-end RNA-sequencing was performed at the Department of Genetics of the University Medical Center Groningen (UMCG). FASTQC (25) quality control was done, and low-quality reads were trimmed with FASTX trimmer (version 0.0.14). TopHat2 (version 0.11.2) (26) alignment was performed using the Ensembl MMul-1 reference genome obtained from Illumina iGenomes. Approximately 10 million high-quality uniquely mapped reads were obtained per sample. The reads were quantified using HT-seq count (27) and imported in R (version 3.2) for differential gene-expression analysis with EdgeR (28). Gene annotation and gene ontology data for the ensemble data were obtained using the R BioMart Bioconductor tool (29). The heat map was generated with log count/million values with heatmap 2. To functionally annotate the differentially expressed gene lists, Ingenuity Pathway Analysis (QIAGEN, Redwood City, CA) was used.

Ags

rhMOG was produced in *Escherichia coli* and purified in house (BPRC), as described (30). In total, 16 synthetic peptides (Table I) were purchased

from Peptide 2.0 (Chantilly, VA) and Pepscan (Lelystad, the Netherlands). Peptides were derived from the MOG sequence of marmosets (Cj-MOGs) and from the MOG sequence of rhesus monkeys (Mm-MOGs). Sequences were downloaded from the National Center for Biotechnology Information protein database (http://www.ncbi.nlm.nih.gov/protein). Note that the MOG34–56 peptides from marmoset and rhesus monkey differ at only one position: a Ser or Pro residue on position 42, respectively. Modifications included substitution of the positively charged Arg residues on positions 41 and 46 (Arg^{41} and/or Arg^{46}) for uncharged Cit.

Magnetic bead assay for proteolytic degradation of MOG peptides

Streptavidin-labeled magnetic beads (Dynabeads; Invitrogen, Carlsbad, CA) were incubated with biotin/FITC-labeled peptides (peptides B1–B8), according to the manufacturer's instructions. Briefly, after a 2-h incubation at room temperature, beads were precipitated with a strong magnet to collect the bound peptides. After two washings of the peptide-coated beads with 160 mM Tris-HCl + 1.6 M NaCl (pH 7.4), they were incubated for 24 h with 40 μl of cell lysates (0.5 mg/ml), 40 μl (CatG) (0.25 mU/μl), or 50 μl of cathepsin H (CatH) (10 ng/μl). After another precipitation step with the magnet, 50 μl of supernatants was collected into a black 96-well plate (Greiner Bio-One, Frickenhausen, Germany). The FITC signal present in the supernatants was measured with a VICTOR^3 Multilabel Counter model 1420 (PerkinElmer, Waltham, MA) to quantify the amount of peptide released from the beads as a measure of proteolysis.

Protease inhibitors

To gain insight into the proteolytic mechanism of B cells, we tested the effect of specific inhibitors of endosomal/lysosomal proteases, including pepstatin A (0.7 mg/ml), specific for aspartyl proteases (cathepsin D [CatD] and cathepsin E); cystatin C (0.7 mg/ml), specific for cysteine proteases (cathepsin B, cathepsin C [CatC], CatH, and cathepsins K, L, and S) and for asparaginyl endopeptidease; and the multifunctional inhibitor cystatin-pepstatin inhibitor (0.7 mg/ml) (31). We used the inhibitor 4-(2-aminoethyl) benzenesulfonyl fluoride hydrochloride (Pefabloc) for the inhibition of serine cathepsins (32). CatG activity was blocked with 0.1 mM Z-glycyl-leucyl-phenyl-chloromethyl ketone (CMK) (33). The inhibitor E64 (*N*-[*N*-(L-3-*trans*-carboxyirane-2-carbonyl)-L-leucyl]-agmatine) (Sigma-Aldrich) is a cysteine peptidase inhibitor with relative selectivity for cysteine cathepsins (34, 35). We used 10 μM E64 to block cysteine cathepsin (CatH) activity in cell lysates.

In all experiments, the cell lysates were incubated for 30 min at 37°C with inhibitors at the indicated concentrations prior to the addition of rhMOG or MOG peptide.

Electrophoresis-based assay for proteolytic degradation of MOG peptides

rhMOG protein (2 μg) or MOG peptides (10 μg) were incubated with cell lysates in 50 mM citrate buffer + 5 mM DTT + 0.1% Triton X-100 (pH 5) in a total volume of 15 μl in Eppendorf tubes. The tubes were incubated for 3, 24, or 48 h at 37°C on an Innova 2000 platform shaker set at 40 rpm. After incubation, 6.25 μl of NuPAGE LDS sample buffer, containing 2.5 μl NuPAGE Sample Reducing Agent (Invitrogen) and 1.25 μl dH_2O, was added to each sample. Subsequently, 18 μl of each sample was loaded onto a 4–12% Bis-Tris gradient gel (Invitrogen). After running for 60–90 min at 135 V, the gels were stained for 3–4 h with Simply Blue Safe Stain (Invitrogen) and destained with dH_2O overnight to visualize the protein/peptide bands. A scan of the gel, which was taken with the ChemiDoc MP Imaging System and Image Lab software (Bio-Rad, Veenendaal, the Netherlands), was used for densitometric analysis. Data in the bar graphs are expressed as percentage of degradation relative to incubations containing rhMOG or MOG peptide only, which were run on the same gel. Calculations were corrected by subtracting the background staining and were normalized by measured area (mm^2).

CatH activity assay

CatH activity in MNC lysates was determined with a commercially available assay (BioVision, Milpitas, CA). Briefly, 50 μl of MNC lysate (200 μg protein/ml) was incubated with CH reaction buffer and CH R-AFC substrate for 24 h at 37°C. Color reaction was measured with the VICTOR^3 Multilabel Counter model 1420 (PerkinElmer) at excitation 405 nm/emission 535 nm. Data are expressed as arbitrary counts. As positive control, 100 ng of active human CatH (BioVision) was used.

CatG activity assay

CatG activity was measured in 50 μl of 200 μg/ml MNC cell lysates in a total volume of 90 μl of 160 mM Tris-HCl + 1.6 M NaCl + 5 mM DTT (pH 7.4) and 10 μl of 200 μM Z-Gly-Gly-Arg-AMC substrate (Bachem, Bubendorf, Switzerland). The total mixture was incubated for 24 h at 37°C, and fluorescence was measured with the VICTOR^3 Multilabel Counter model 1420 (PerkinElmer) at an excitation wavelength of 355 nm and an emission wavelength of 460 nm. As positive control, 5 mU/ml human CatG (Sigma-Aldrich) was used.

Quantitative PCR

Total RNA was extracted from PBMCs and spleen MNCs, and cDNA was synthesized for quantitative PCR (qPCR) using primer–probe combinations (Table II) according to the Universal Probe Library (Roche, Indianapolis, IN), as previously described (24). Transcript levels were normalized against the reference gene Abelson (ABL). Only cathepsin mRNA transcripts were analyzed for which reliable primer–probe combinations could be designed.

Western blotting for LC3

BLCs and splenocytes (10^6 cells) from *C. jacchus* and *M. mulatta* were incubated overnight at 37°C with 500 nM bafilomycin (Sigma-Aldrich) to prevent maturation of autophagic vacuoles by inhibiting fusion between autophagosomes and lysosomes. Cells were harvested in Eppendorf tubes and, after a short spin (10,000 rpm), cell pellets were resuspended in 40 μl of culture media (RPMI 1640 without FCS) and frozen at −80°C for ≥3 h. After thawing of cell suspensions, 2 μl of 500 U/ml Benzonase Nuclease (Merck Millipore, Amsterdam, the Netherlands) was added to degrade all forms of DNA and RNA, followed by sonification in a sonic water bath (6 × 30 s with 30-s intervals) while cooling on ice. Six microliters of each sample was solubilized in 6 μl Laemmli sample buffer containing 0.3 μl of 50 mM 2-ME (Bio-Rad), and 10 μl was loaded on a mini PROTEAN TGX stain-free 4–20% gel (Bio-Rad), which was run for 35 min at 200 V. As a positive

Table I. Peptide sequences

Species	Code	Peptide Name	Sequence
Marmoset/mouse	A1	Cj-MOG35–51	MEVGWYRSPFSRVVHLY
	A2	Cj-MOG34–51 Cit41	MEVGWY-Cit-SPFSRVVHLY
	A3	Cj-MOG34–51 Cit46	MEVGWYRSPFS-Cit-VVHLY
	A4	Cj-MOG34–51 Cit41+46	MEVGWY-Cit-SPFS-Cit-VVHLY
Rhesus/human	A5	Mm-MOG35–51	MEVGWYRPPFSRVVHLY
	A6	Mm-MOG34–51 Cit41	MEVGWY-Cit-PPFSRVVHLY
	A7	Mm-MOG34–51 Cit46	MEVGWYRPPFS-Cit-VVHLY
	A8	Mm-MOG34–51 Cit41+46	MEVGWY-Cit-PPFS-Cit-VVHLY
Marmoset/mouse	B1	Cj-MOG35–51	Biotin-MEVGWYRSPFSRVVHLYK-FITC
	B2	Cj-MOG34–51 Cit41	Biotin-MEVGWY-Cit-SPFSRVVHLYK-FITC
	B3	Cj-MOG34–51 Cit46	Biotin-MEVGWYRSPFS-Cit-VVHLYK-FITC
	B4	Cj-MOG34–51 Cit41+46	Biotin-MEVGWY-Cit-SPFS-Cit-VVHLYK-FITC
Rhesus/human	B5	Mm-MOG35–51	Biotin-MEVGWYRPPFSRVVHLYK-FITC
	B6	Mm-MOG34–51 Cit41	Biotin-MEVGWY-Cit-PPFSRVVHLYK-FITC
	B7	Mm-MOG34–51 Cit46	Biotin-MEVGWYRPPFS-Cit-VVHLYK-FITC
	B8	Mm-MOG34–51 Cit41+46	Biotin-MEVGWY-Cit-PPFS-Cit-VVHLYK-FITC

Table II. Primers with corresponding probes used for qPCR

Species	Gene	5′–3′ Primer	3′–5′ Primer	Probe
	ABL	CAGAGAAGGTCTATGAACTCATGC	GGTGGATTTCAGCAAAGGAG	86
Marmoset	CatB	GGGAGCCTTCTCTGTGTACG	CTCGCCAGTGACATGCTG	4
	CatC	CGATGTCAACTGCTCGGTTA	AATTGCCAAGGTCATCATACG	131
	CatD	TCCCTGTTCTACCTGAACGTC	GTCCACAATGGCCTCACAG	39
	CatF	CCCAGGACTTGGCTGTGA	CGGTTATAGGTAATGACAAAGTTCC	135
	CatG	TTTGTGCTAACAGCAGCTCAC	CTGGGTCCTTTCCCGTCT	60
	CatH	ATGGGCGAAGACACCTACC	TTTCCGGGCTGGAACTTAC	37
	CatK	CCGGGGTATTGATTCTGAAG	GCCTTGCCTGTTGGGTTAT	63
	CatL2	CAATGGGGAATACAGCCAAG	CAAACCATCACCTGCCTGA	135
	CatO	CAGCAGATGTGTGGAGGATG	GGCTTTCCTTTTATCGCACA	86
	CatS	GGGTGTGTTACCGAAGTGAAA	CCCCCACAGCACTGAAAG	40
	PAD2	GCAGGAGAACCTGTACTTCCA	GCAGGTCAATGATGTCCTGTT	17
	PAD4	TACACTCACCGTCTCCATGC	CCACACTGTCTTGGAACAACA	1
Rhesus monkey	CatB	CAGTGTCCCACCATCAAAGA	ATGCAGATCCGGTCAGAGAT	54
	CatC	TGACTACAAGTGGTTTGCCTTTT	TTGTCTCATTGCAGTAAATGGTC	148
	CatD	AACTGCTGGACATCGCTTG	GCAAATGAGGTGCCATTCTT	22
	CatE	AGCTGCAAAATGCCATCG	TGGCACACTCCACAGCATA	58
	CatG	GCGAGACAACTTTGTGCTGA	TCCCGTCTCCGGATATTGT	60
	CatH	GGGATCATGGGTGAAGACAC	CTTTCCAGGCCGGAACTT	37
	CatK	CTGGGTTTGATAAAACAGGTAACA	TGGGCGTAACCATCTACTCC	60
	CatL2	CAATGGGGAATACAGCCAAG	AACCCATCACCTGCCTGA	135
	CatO	CTGGGTTTGATAAAACAGGTAACA	TGGGCGTAACCATCTACTCC	60
	CatW	TTTGGGGTGACTCCATTCAG	CTCCGATACCCGTAGAGCTG	63
	PAD2	CCTCCTGTGTCGGTGTTTG	GAAGCAGACCTTCAGGTCACA	22
	PAD4	TGAGAGAACATAATTCATTTGTGGA	CGGAATGTCGATGATGTCAC	24

control, LC3-I and LC3-II were loaded onto the gel, which were provided together with the anti-LC3 Ab (nanoTools, Teningen, Germany). The Bio-Rad Trans-Blot Turbo Transfer System was used for blotting the gels onto a 0.2-μm polyvinylidene difluoride membrane (predefined program: Low MW). Samples were immunoblotted with mouse anti-LC3 (clone 5F10; nanoTools; dilution 1:200) and with goat anti-GAPDH as loading control (Novus, Abingdon, U.K.; dilution 1:1,000) in Animal-Free Blocker (Vector Laboratories, Burlingame, CA) overnight at 4°C. Rabbit anti-mouse–HRP (Dako, Glostrup, Denmark; dilution 1:1,000) and mouse anti-goat–HRP (Jackson ImmunoResearch, Newmarket, U.K.; dilution 1:100,000) in Animal-Free Blocker were used as secondary Abs. Blots were incubated for 1 h at room temperature and developed using Clarity Western ECL substrate (Bio-Rad). A ChemiDoc MP Imaging System and Image Lab software (Bio-Rad) were used to visualize and quantify the density of the bands. LC3-I and LC3-II bands were normalized against GAPDH.

Immunofluorescence staining

Mm-BLCs, marmoset BLCs (Cj-BLCs), total marmoset SCs (Cj-SCs), total Mm-SCs, $CD20^+$ cells, and $CD20^-$ cells were washed with PBS, and cytospins (35,000 cells/slide) were made with the Cytospin 4 Cytocentrifuge (ThermoFisher Scientific). Cells were permeabilized for 20 s with −20°C methanol, air dried, and incubated with the following primary Abs in PBS/1% BSA for 1 h at room temperature: anti-rabbit PAD2 (1:28; ab16478; Abcam, Cambridge, U.K.), anti-rabbit PAD4 (1:10; PA5-22317; Invitrogen), and anti-mouse LC3 (1:250; clone 5F10; nanoTools). Cells were washed three times with PBS and incubated with the secondary Ab goat anti-rabbit IgG/FITC (1:200; KPL) or chicken anti-mouse IgG/Alexa Fluor 594 (1:2000; ThermoFisher Scientific) and with DAPI (1:1000) for 1 h at room temperature in PBS/1% BSA. After four final wash steps with PBS, coverslips were mounted with the antifade solution Citifluor AF-1 (Agar Scientific, Essex, U.K.). Imaging was performed with a Nikon Microphot-FXA microscope (Tokyo, Japan) with a 40× lens and a digital camera (Nikon FX-35DX).

Results

Comparative RNA sequencing of LCV-infected and noninfected B cells

We performed RNA sequencing to examine changes in molecular pathways induced in *M. mulatta* B cells upon immortalization by experimental infection with the LCV HV papio. The analysis included four samples: HV papio–immortalized Mm-BLCs, $CD20^+$ B cells isolated from rhesus monkey PBMCs (Mm-PBMCs), the residual $CD20^-$ PBMC fraction, and unsorted Mm-PBMCs. Three main analyses were performed: principal component analysis (PCA) to determine the similarity between the biological replicates for each condition and the differences among conditions; differential gene-expression analysis to identify gene differences among conditions; and Ingenuity Pathway Analysis to identify pathways and gene categories that are overrepresented in the differential gene-expression analyses (Fig. 1).

PCA (Fig. 1A) shows close clustering of the expression profiles of the three biological replicates within each condition, indicating that they are highly similar, as was expected. The figure also shows that the first principal component clearly distinguishes Mm-BLCs from the other samples. The primary aim of the differential gene-expression analysis was to identify genes that were differentially expressed between HV papio–infected and noninfected *M. mulatta* B cells. The most relevant comparison for the current study is Mm-BLCs versus $CD20^+$ Mm-PBMCs (Fig. 1B). In total, 3108 (1055 + 2053) genes were expressed at a significantly higher level in Mm-BLCs compared with $CD20^+$ *M. mulatta* B cells, and 2721 (1087 + 1634) genes were expressed at a significantly lower level (false discovery rate, $p < 0.01$; logFC > 1). Furthermore, we observed a strikingly high overlap between Mm-BLCs and the $CD20^-$ Mm-PBMC fraction (2053 and 1634 up- and downregulated genes in common, respectively).

We were particularly interested in genes related to the Ag processing and presentation pathways, including the vacuolar route via endolysosomes and the cytosolic route via the proteasome (17). Using Gene Ontology categories, all genes that were differentially expressed between Mm-BLCs and $CD20^+$ Mm-PBMCs were depicted as a heat map (Fig. 1C). Individual genes with their fold change (BLC versus $CD20^+$, BLC versus $CD20^-$, and $CD20^+$ versus $CD20^-$) are listed in Supplemental Table I.

Gene candidates of interest are CIITA and NLRC5, the master regulators of MHC class II and MHC class I expression, respectively (36, 37), which are both downregulated in HV papio–infected *M. mulatta* B cells. Several costimulatory molecules were upregulated, such as CD80, TNFSF4 (Ox40L), CD70, and Fas ligand. Others were downregulated, such as CD40, CD86, and PDCD1 (PD1). Moreover, a number of cathepsins were differentially expressed.

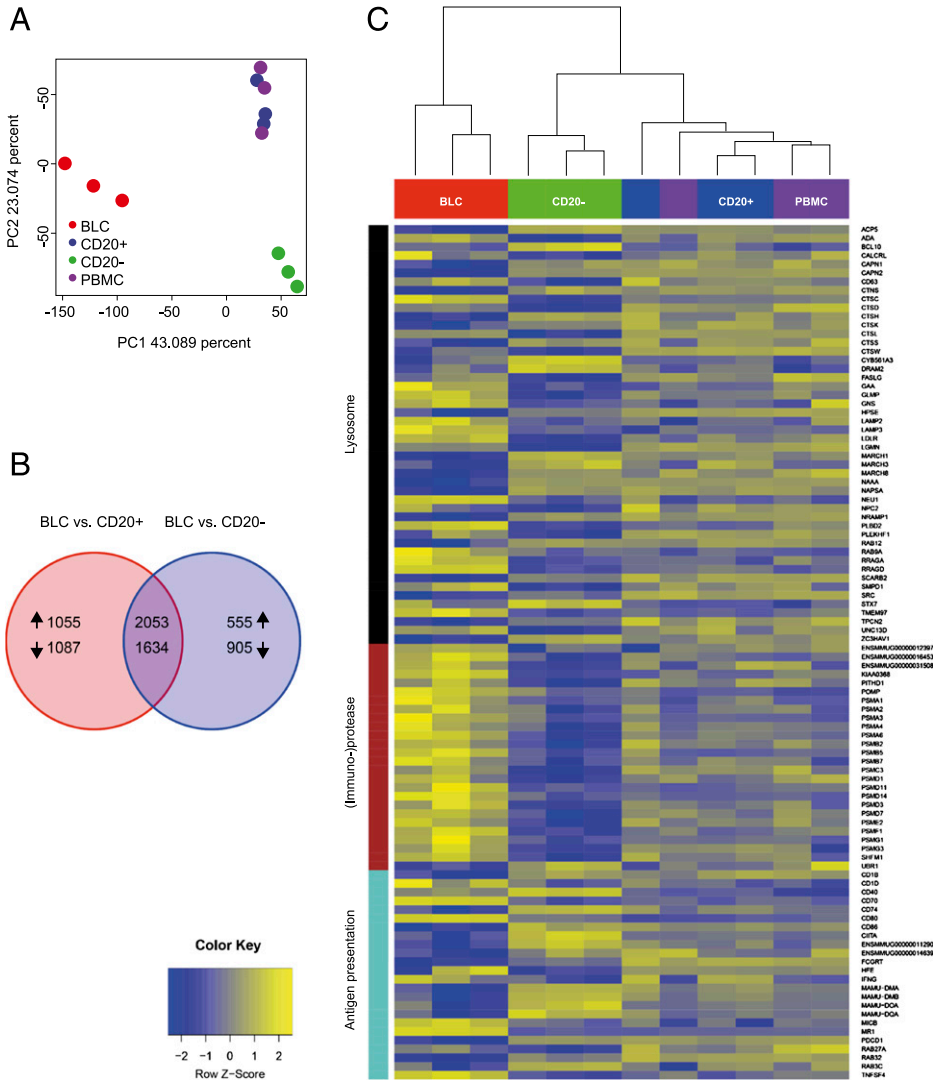

FIGURE 1. RNA sequence data. High-throughput Illumina single-end sequencing was performed on three replicates of BLC, CD20$^+$, CD20$^-$, and PBMC samples. (**A**) PCA was done on the samples, and the first and second components are depicted as a scatter plot. (**B**) Differential gene-expression analysis was performed on BLCs versus CD20$^+$ and BLCs versus CD20$^-$, and the number of differentially expressed genes (false discovery rate $<$ 0.01, logFC $>$ 1) is depicted as a Venn diagram. (**C**) In these differential gene-expression lists, selected genes associated with Ag presentation, lysosome, and proteasome are depicted as a sample clustered heat map with Z-scores across samples. A list of all genes with their fold change (BLC versus CD20$^+$, BLC versus CD20$^-$, and CD20$^+$ versus CD20$^-$) is shown in Supplemental Table I.

Lastly, a plethora of proteasome-related genes were consistently upregulated in HV papio–infected *M. mulatta* B cells.

Taken together, the RNA-sequencing data indicate that HV papio infection of *M. mulatta* B cells induces a unique gene-transcription profile that clearly differs from noninfected CD20$^+$ *M. mulatta* B cells. Differentially transcribed genes include those associated with Ag presentation and with proteasome and endolysosome functions; however, the most significantly upregulated pathways relate to enrichment of cell cycle and cholesterol biosynthesis.

Transcription profiles and activity of cathepsin in APC subsets

Cathepsins are proteases of the endolysosomal pathway that are centrally involved in the processing of protein Ags (38). We analyzed mRNA transcript profiles for a number of cathepsins in total PBMCs or SCs, the CD20$^+$ and CD20$^-$ SC subfractions, and BLCs generated from marmosets and rhesus monkeys. Because we were unable to isolate sufficient numbers of CD20$^+$ Cj-SCs from the small-bodied marmosets, we only included unfractionated Cj-PBMCs and Cj-SCs, as well as Cj-BLCs, from that species.

Isolates of mRNA from unfractionated, CD20$^-$ and CD20$^+$ Mm-SCs, and Mm-BLCs were analyzed by qPCR. Fig. 2A shows that CatG mRNA is barely detectable in CD20$^+$ Mm-SCs and that transcript levels did not change postinfection with HV papio. This contrasts with data obtained in humans: detectable levels of CatG protease activity were found in CD20$^+$ cells (39). In the CD20$^+$ Mm-SC fraction (i.e., B cells), CatH also attracted our attention because the mRNA transcript level of this cysteine protease was highly expressed in *M. mulatta* B cells but was downregulated postinfection with HV papio. This downregulation by LCV infection was also observed in the RNA-sequencing analysis. In addition, we found increased mRNA transcripts of the cysteine protease CatC in HV papio–infected *M. mulatta* B cells.

Because the data from marmoset Cj-SCs and EBV–B95-8–induced Cj-BLCs essentially mirrored those obtained in the corresponding fractions from rhesus monkeys, with the exception of CatD and cathepsins K and O (Fig. 2B), we assume that values obtained for the other cathepsins in CD20$^+$ and CD20$^-$ SC fractions from rhesus monkeys may be tentatively extrapolated to marmosets.

Proteolytic degradation of rhMOG in SC lysates from marmosets and rhesus monkeys

We analyzed the degradation of rhMOG in lysates from Cj-SCs and Mm-SCs to examine potential species-related differences. To this end, rhMOG was incubated for 3, 24, and 48 h with different doses of cell lysates. Fig. 3A–C show intact rhMOG as a single band of ±19 kDa in the gel. Full degradation of rhMOG with the highest concentration (5 μg) of Cj-SC lysate was detected after 48 h of incubation; however, its degradation by Mm-SC lysate was incomplete under these conditions. The pattern of bands suggests that rhMOG may be cleaved at different positions in Mm-SCs

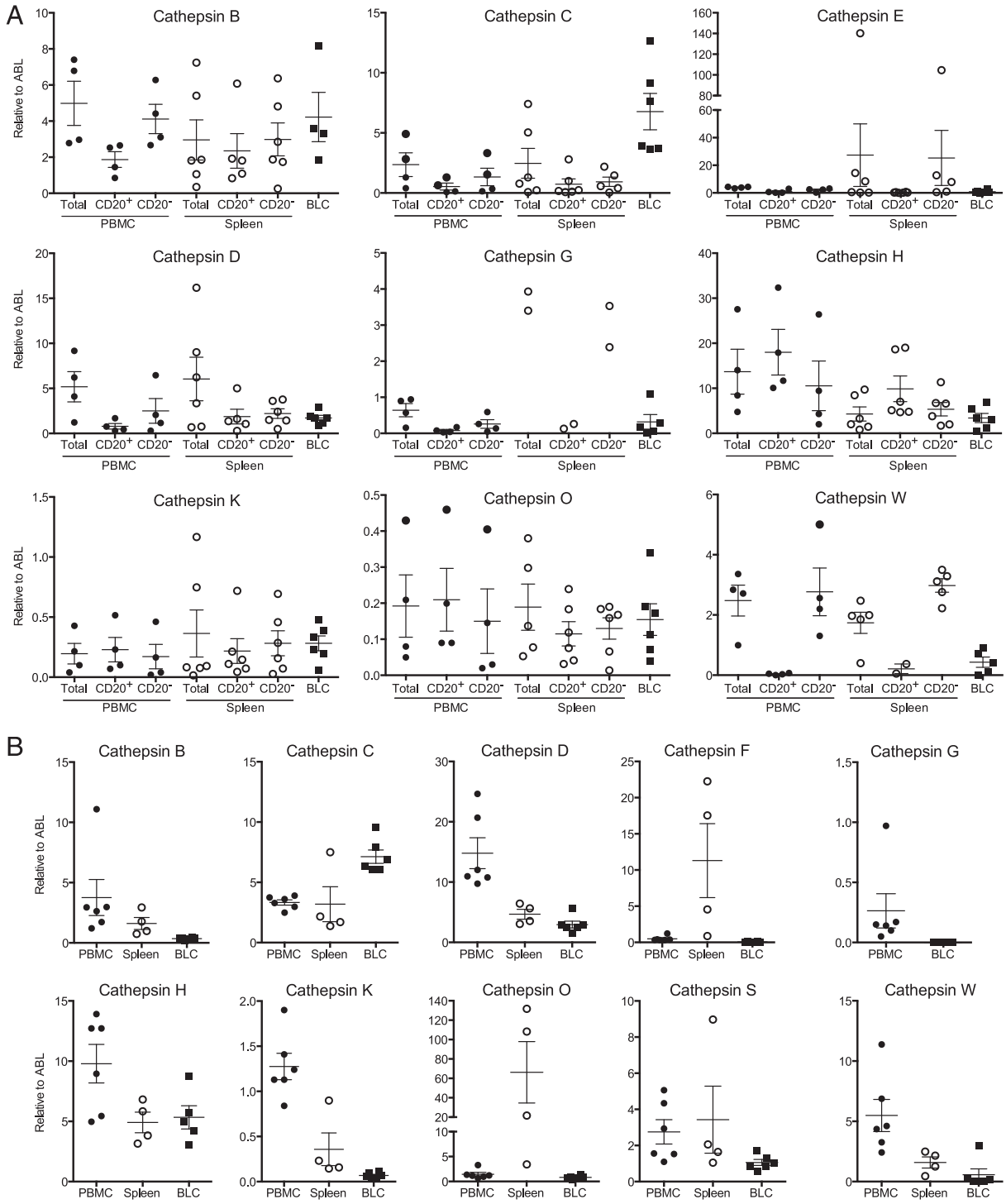

FIGURE 2. qPCR of cathepsin transcripts in MNC subsets from rhesus monkey and marmosets. Total RNA was extracted from rhesus monkey (**A**) and marmoset (**B**) PBMCs and spleen MNCs. Also, $CD20^+$ and $CD20^-$ fractions were isolated from rhesus monkey samples. cDNA was synthesized for qPCR using primer–probe combinations (Table II). Transcript levels were normalized against ABL. Data are presented as mean ± SEM.

compared with Cj-SCs. The observation that degradation is slower in Mm-SCs than in Cj-SCs, with the persistence of intermediate degradation products being observed in Mm-SCs, indicates that processing of rhMOG may be different between rhesus monkeys and marmosets.

To test whether B cell proteases contribute to the proteolytic degradation of rhMOG, we incubated the protein with lysates from the $CD20^-$ and $CD20^+$ fractions of Mm-SCs for 3, 24, and 48 h. Fig. 3D–F show that rhMOG was rapidly and completely degraded in lysates from the $CD20^-$ fraction of Mm-SCs, whereas only moderate degradation could be detected in the $CD20^+$ fraction.

Regarding the prominent role of LCV-infected B cells as APCs in the nonhuman primate EAE models (12), we also tested proteolytic degradation of rhMOG in lysates of BLCs. BLCs were generated by infecting marmoset and rhesus monkey MNCs with the relevant LCV (i.e., human EBV–B95-8 and HV papio, respectively). Fig. 3G–I demonstrate that rhMOG is minimally degraded in lysates of rhesus monkey or marmoset BLCs, although some degradation products could be distinguished as smaller

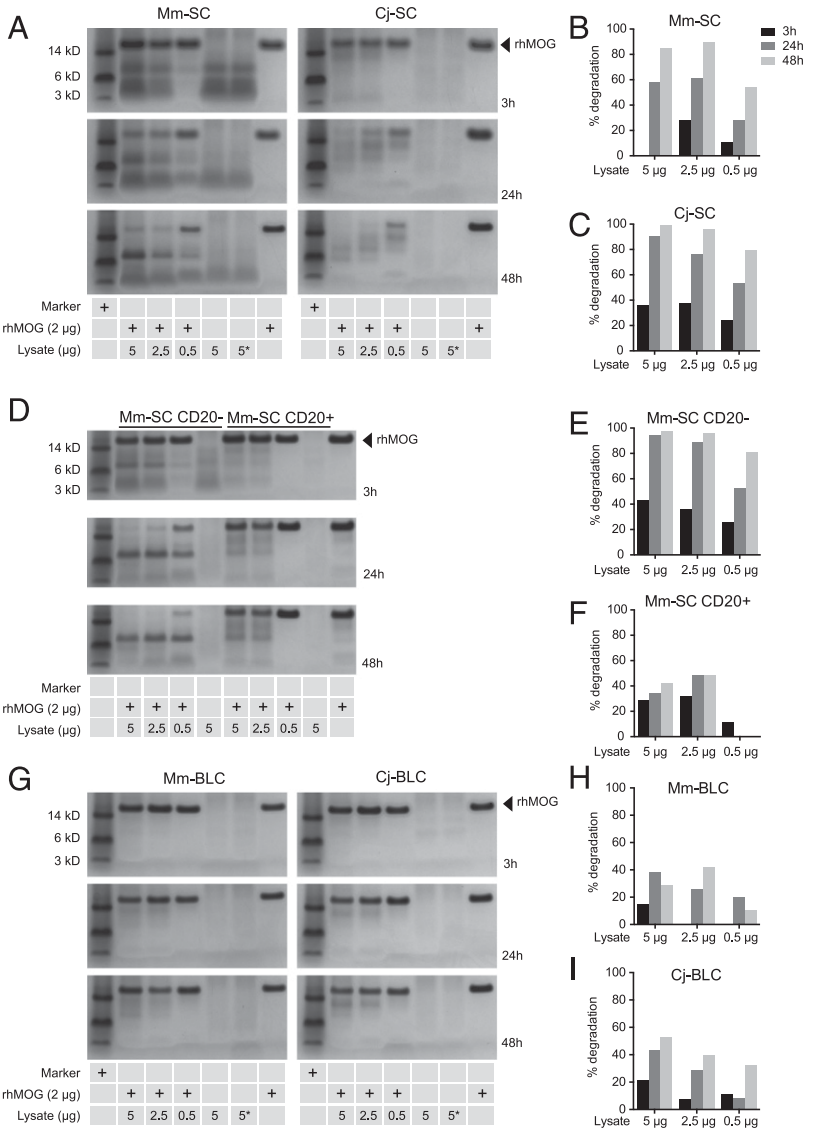

FIGURE 3. Proteolytic degradation of rhMOG. A fixed concentration (2 μg/ml) of rhMOG was incubated for 3, 24, or 48 h with different concentrations (5, 2.5, and 0.5 μg) of lysates from Mm-SCs and Cj-SCs (**A**), Mm-SC CD20$^+$ and Mm-SC CD20$^-$ fractions (**D**), and Mm-BLC and Cj-BLC lysates (**G**). After the indicated time intervals aliquots of the lysates were run on a 4–12% Bis-Tris gradient gel, which was stained with Coomassie Blue to visualize degradation. For each gel, the percentage degradation of rhMOG was calculated as described in *Materials and Methods*. The percentage degradation of rhMOG by the different lysates is shown for Mm-SCs (**B**), Cj-SCs (**C**), Mm-SC CD20$^+$ (**E**), Mm-SC CD20$^-$ (**F**), Mm-BLCs (**H**), and Cj-BLCs (**I**). Second to last lane contained lysate with OVA as an irrelevant Ag. OVA was not degraded and is not shown in this figure. Data shown are a representative of at least three replicates.

bands in the Cj-BLC incubate at 48 h. These data indicate that, although B cells are capable of proteolytic degradation of rhMOG, this activity is nearly completely abolished by infection with LCV.

Delineating the roles of CatG and CatH

Data reported by Burster et al. (39) show a central role for CatG in the processing of the myelin Ag myelin basic protein in human B cells. However, the qPCR data in Fig. 2A show high levels of CatG mRNA in CD20$^-$ SCs, whereas it was undetectable in CD20$^+$ SCs. Because the absence of (active) CatG protein may well explain the different degree of rhMOG degradation in both fractions, we examined the effect of the specific CatG inhibitor CMK. Because the qPCR data in Fig. 2 show that CatH mRNA expression in B cells is downregulated after LCV infection, we also included CatH in this analysis, a protease with aminopeptidase and endopeptidase activity that can also cleave peptides at Arg residues (40, 41). Because a specific inhibitor of CatH is not available, we used the covalent cysteine cathepsin inhibitor E64. Note that E64 is not specific for CatH; at the concentrations used, it also inhibits the other cysteine cathepsins.

First, we tested the level of CatG and CatH activity in the different cell lysate preparations using protease-specific assay kits; for validation purposes, the inhibitors CMK and E64 were included. The data in Fig. 4A show that considerable CatG activity was detected in all analyzed cell preparations and that activity could be inhibited to background level with CMK; E64 had no effect on CatG activity (data not shown). The highest CatG activity was observed in BLCs from marmosets and rhesus monkeys and in CD20$^-$ Mm-SCs. All assayed cell preparations also tested positively for CatH activity, which could be inhibited with the nonspecific cysteine cathepsin inhibitor E64; CMK had no effect in the CatH assay (data not shown). The highest CatH activity was detected in the lysate of unfractionated Cj-SCs; it was approximately twice as high as the activity in Mm-SCs.

To confirm the involvement of CatG and CatH in the degradation of rhMOG, we tested the effect of E64 and CMK on rhMOG degradation in lysates of CD20$^+$, CD20$^-$, and unfractionated Mm-SCs. Fig. 4B and 4C show that the degradation of rhMOG in lysates of nonfractionated Mm-SCs or CD20$^-$ Mm-SCs was only partially inhibited by CMK or E64, whereas the degradation of rhMOG in the CD20$^+$ Mm-SC lysate was reduced to background levels. Interestingly, Fig. 4D and 4E show that the degradation of rhMOG in the lysate of nonfractionated Cj-SCs was almost completely suppressed by CMK and E64.

In conclusion, the data indicate an active role for CatG and probably for CatH in the proteolytic degradation of rhMOG.

Degradation of MOG35–51 in cell lysates of rhesus monkeys and marmosets

The specificity profile of CatG from rhesus monkeys and marmosets differs. Although CatG from both species has chymotryptic

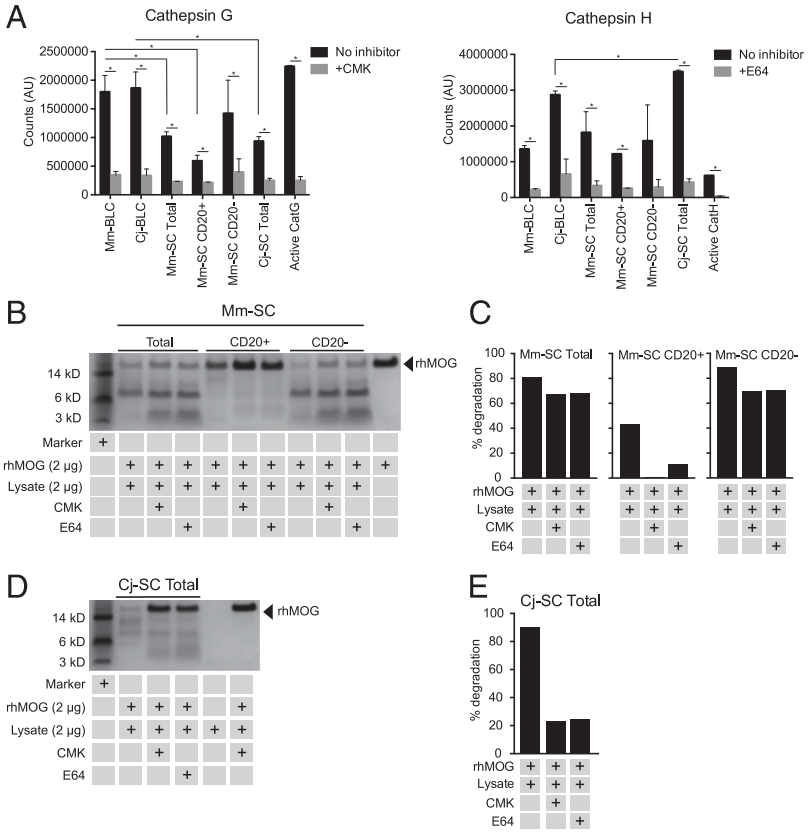

FIGURE 4. Involvement of CatG and CatH in rhMOG degradation. (**A**) Activity measurements of CatG (left panel) and CatH (right panel) in the indicated cell lysates. Measurements were performed in the absence or presence of the inhibitors CMK and E64. Data are presented as mean ± SEM. Lysates were prepared from total Mm-SCs, as well as from $CD20^-$ and $CD20^+$ cell fractions. (**B**) Lysates were incubated with rhMOG for 24 h in the presence or absence of CMK or E64. (**C**) Percentage degradation of rhMOG. (**D** and **E**) The same analysis was performed for nonfractionated Cj-SCs. Data shown are a representative of at least three replicates. $*p < 0.05$.

activity, cleaving at aromatic residues (Trp, Phe, Tyr), rhesus monkey and human CatG also have tryptic activity and can cleave after Lys and Arg residues (42).

The pathogenically dominant MOG epitope 40–48 (**YR**PP**F**S**R**VV) contains four potential CatG cleavage sites: the two Arg residues at position 41 and 46 and the aromatic residues Tyr (Y40) and Phe (F44) (Fig. 5). This was confirmed when we incubated the longer peptide MOG35–51 with human CatG and analyzed the generated fragments with mass spectrometry (data not shown). Therefore, we reasoned that CatG destroys the pathogenically highly important MOG40–48 epitope during processing in B cells.

For the initial analyses of MOG peptide proteolysis we used magnetic beads coated with MOG35–51 peptides. Alignment of the peptide sequences from a variety of species ranging from the naked mole rat to human shows the high conservation of this sequence; only position 42 is bimorphic and can be occupied by a Ser (S) or Pro (P) residue (Fig. 5). We first tested whether the presence of a Ser or Pro residue at position 42 alters the degradation of the MOG peptide. To this end, we incubated peptide-coated magnetic beads for 24 h with variable concentrations of lysates from $CD20^+$ and $CD20^-$ Mm-SCs in the presence of cathepsin inhibitors. Fig. 6 shows moderate cleavage of the marmoset peptide (Cj-MOG35–51) in the $CD20^+$ Mm-SC fraction lysate, which already reached a plateau at a lysate concentration of 4 μg/ml, whereas degradation of the rhesus monkey peptide (Mm-MOG35–51) increased in a dose-dependent fashion. In the $CD20^-$ fraction, degradation of the rhesus monkey peptide (Mm-MOG35–51) was approximately three times higher than degradation of the marmoset peptide (Cj-MOG35–51). Proteolytic activity in the $CD20^+$ fraction was reduced to background levels by the general serine protease inhibitor Pefabloc and the CatG-specific inhibitor CMK. The other inhibitors exerted no detectable effect, indicating that the serine protease CatG has an exclusive role in the degradation of the MOG35–51 peptides in the B cell lysate. In the $CD20^-$ fraction, lysate cleavage was inhibited by Pefabloc, but not by CMK, indicating that CatG is not involved but that the peptides are degraded by other serine proteases that need to be identified.

We used the same assay for testing the proteolytic degradation of the two MOG peptides in BLC lysates. Fig. 6B shows that the two MOG peptides (Cj-MOG35–51 and Mm-MOG35–51) are more or less equally degraded in Mm-BLC lysate and that degradation is completely suppressed by the inhibitor CMK. Also, the two peptides are equally degraded in lysate of marmoset Cj-BLCs; however, in this case, the inhibitor CMK was only partially effective. The inhibitor E64 had no effect in this assay, indicating that CatG is the principal protease for degradation of the peptide.

In the next set of experiments, degradation of the MOG peptide was confirmed on an SDS-PAGE gel. Fig. 7A and 7B show that about 80% of the Cj-MOG35–51 and Mm-MOG35–51 peptides was degraded in lysates of total Mm-SCs and of the $CD20^+$ and $CD20^-$ fractions. The inhibitors CMK and E64 were not equally effective in all conditions. The CatG inhibitor CMK reduced degradation of the Mm-MOG35–51 peptide in the total Mm-SC lysate more effectively than that of the Cj-MOG35–51 peptide. However, in the $CD20^+$ SC fraction, the suppressive effect of E64 on the degradation of both peptides was substantially higher than the effect of CMK. E64 incompletely inhibited the degradation of the Mm-MOG35–51 peptide in the $CD20^-$ fraction lysate, whereas degradation of the Cj-MOG35–51 peptide was completely inhibited. These observations suggests that the partial inhibitory effect of CMK observed in the Cj-BLC lysate (Fig. 6B) may be due to residual activity of CatH. Indeed, the CatG inhibitor CMK reduced the degradation of both peptides in the Cj-SC lysate to ∼50%. In the experiment depicted in Fig. 7C and 7D, the degradation of both peptides was tested in unfractionated Cj-SC lysates. The data show that degradation of the Cj-MOG35–51 peptide was suppressed less effectively by

	1 10	20	30 #	40	50	60
Human	GQFRVIGPRH	PIRALVGDEV	ELPCRISPGK	NATGMEVGWY	RPPFSRVVHL	YRNGKDQDGD
Rhesus	GQFRVIGPRQ	PIRALVGDEV	ELPCRISPGK	NATGMEVGWY	RPPFSRVVHL	YRNGRDQDGE
Marmoset	GQFRVIGSRH	PIQALVGDAA	ELPCRISPGK	NATGMEVGWY	RSPFSRVVHL	YRNGKDQDGE
Mouse	GQFRVIGPGY	PIRALVGDEA	ELPCRISPGK	NATGMEVGWY	RSPFSRVVHL	YRNGKDQDAE
Rat	GQFRVIGPGH	PIRALVGDEA	ELPCRISPGK	NATGMEVGWY	RSPFSRVVHL	YRNGKDQDAE
Naked mole rat	GQFQVVGPAH	PLRALVGDAV	ELPCRISPGK	NASGMEVGWY	RPPFSRVVHL	YRQGRDQDAE

	70	80	90	100	110	120	125
Human	QAPEYRGRTE	LLKDAIGEGK	VTLRIRNVRF	SDEGGFTCFF	RDHSYQEEAA	MELKVEDPFY	WVSPG
Rhesus	QAPEYRGRTE	LLKDAIGEGK	VTLRIRNVRF	SNEGGFTCFF	RDHSYQEEAA	IELKVEDPFY	WVSPA
Marmoset	QAPEYRGRTE	LLKDDIGEGK	VTLKIRNVRF	PDEGGFTCFF	RDHSYQEEAA	MQLKVEDPFY	WVSPG
Mouse	QAPEYRGRTE	LLKETISEGK	VTLRIQNVRF	SDEGGYTCFF	RDHSYQEEAA	MELKVEDPFY	WVNPG
Rat	QAPEYRGRTE	LLKESIGEGK	VALRIQNVRF	SDEGGYTCFF	RDHSYQEEAA	VELKVEDPFY	WINPG
Naked mole rat	QAPEYRGRTE	LLTEAIGEGK	VTLRIRNVRF	SDEGGFTCFF	RDHSYQEEAA	VALKVEDPFY	WISPG

FIGURE 5. Alignment of recombinant MOG sequences. Recombinant MOG sequences encoding from 1 to 125 were aligned for the following species: human, rhesus monkey, marmoset, mouse, rat, and naked mole rat. The pathogenically relevant T cell epitope in the rhMOG sequence MOG24–36 (MHC class II/Caja-DRB1*W1201–binding Th1 epitope) is single underlined, whereas the one in MOG40–48 (MHC class I/Caja-E–binding NK-CTL epitope) is double underlined. The two epitopes are located in close proximity within the highly conserved sequence 21–58. The only difference between the sequence in mouse/marmoset/rat versus rhesus monkey/human MOG is a substitution of proline (P) by a serine (S) at position 42 (indicated in green). The Arg (R) residues, which can be citrullinated by posttranslational modification, are indicated in red. The pound sign (#) marks the only N-glycosylation site at the asparagine (N) at position 31.

CMK than was degradation of the Mm-MOG35–51 peptide, whereas the cysteine cathepsin inhibitor E64 was about equally effective.

Finally, we also tested the proteolytic degradation of the two peptides in lysates of LCV-infected B cells from the two species. Fig. 7D and 7E show that the degradation of both peptides is about equally effective in Mm-BLCs and Cj-BLCs and that the inhibitors CMK and E64 were about equally effective.

In conclusion, the presence of a Ser or Pro residue on position 42 has no clear influence on the sensitivity of MOG35–51 peptide to proteolytic degradation in B cell lysates. Both assays show a clear role for CatG in the degradation of the peptide.

Degradation of citrullinated MOG35–51 peptides in cell lysates

Because CatG is prominently involved in the degradation of rhMOG in B cells and has a preference for Arg residues at the cleavage site, we hypothesized that substitution of the Arg[41] and/or Arg[46] residues by neutrally charged Cit might affect the degradation of the peptides in BLC lysates. Fig. 8A shows a major effect of Arg substitution by Cit on the degradation of the MOG peptides, although the effect differed remarkably between the Cj-MOG35–51 and Mm-MOG35–51 peptides. Replacement of the Arg[41] or Arg[46] residue or both for Cit did not alter the sensitivity of the Mm-MOG35–51 peptide to

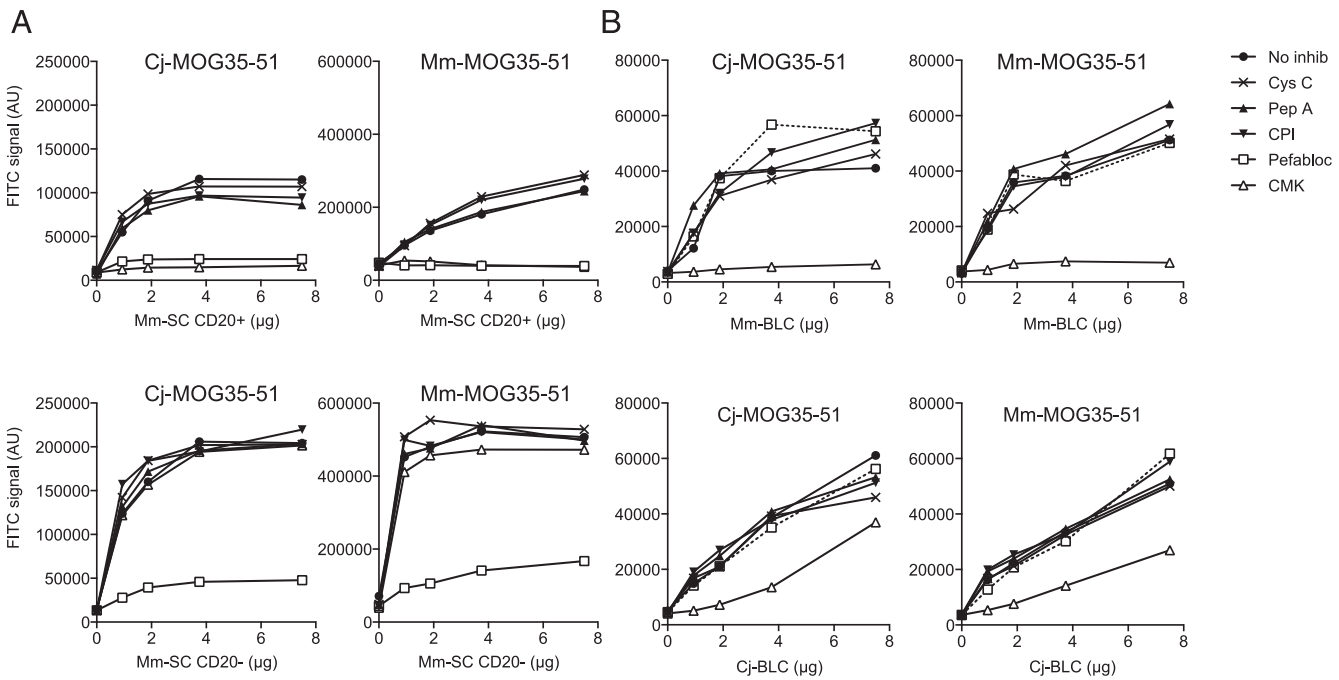

FIGURE 6. Degradation of bead-coated Mm-MOG35–51 and Cj-MOG35–51. Peptides that were labeled at the N terminus with biotin and at the C-terminal end with FITC were coated on magnetic beads via streptavidin. The peptide-coupled beads were incubated for 24 h at 37°C in lysates of $CD20^+$ (upper panel) and $CD20^-$ (lower panel) SC fractions from rhesus monkeys (**A**) or Mm-BLCs (upper panel) and Cj-BLCs (lower panel) (**B**). The indicated inhibitors were tested at the optimal concentration. Depicted is the release of FITC in arbitrary units (AU) from the peptide into the supernatant, as a measure of proteolytic activity.

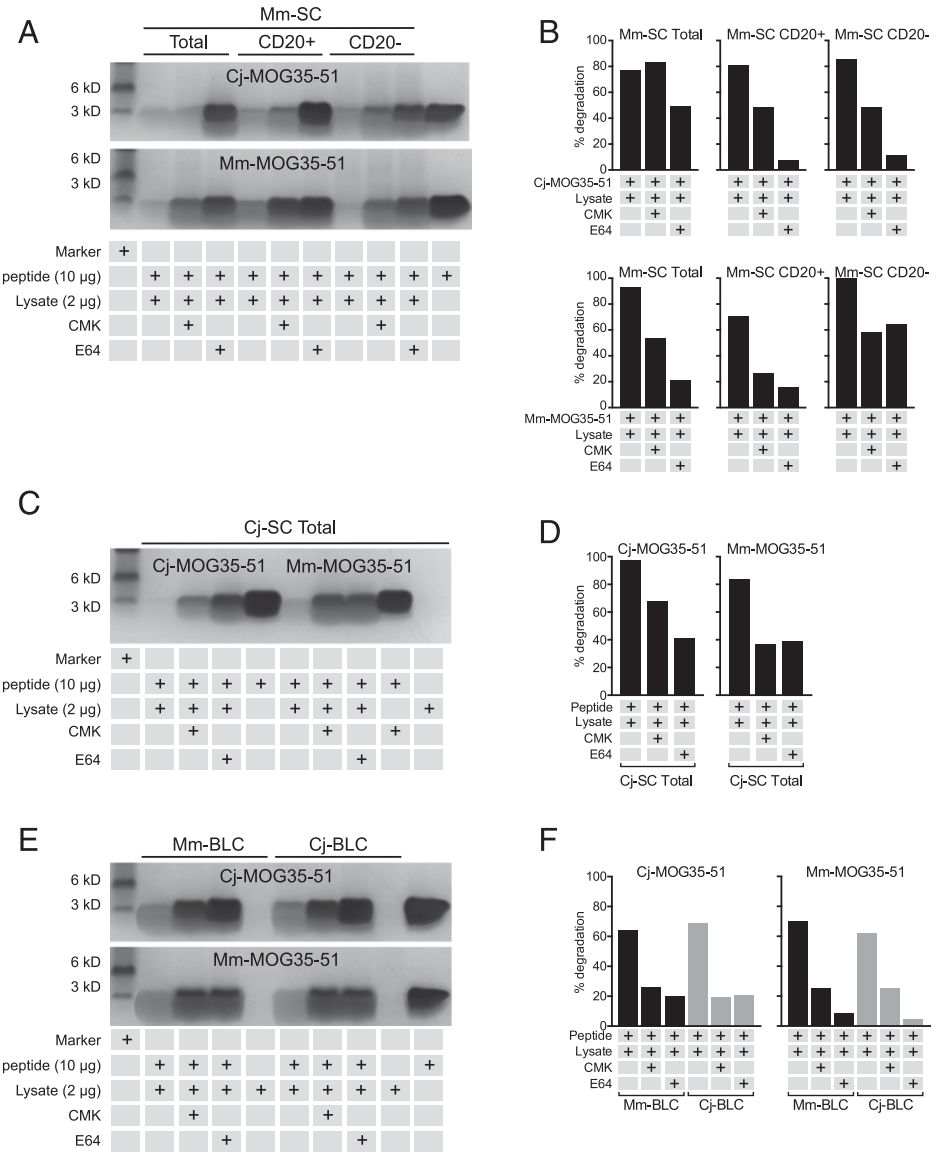

FIGURE 7. Mm-MOG35–51 and Cj-MOG35–51 degradation by different cell lysates. (**A**) Cj-MOG35–51 and Mm-MOG35–51 peptides were incubated for 24 h at a fixed concentration (10 μg/ml) with total SC lysate and with $CD20^+$ and $CD20^-$ spleen fractions from rhesus monkeys. (**B**) Percentage degradation of the MOG peptides. Total Cj-SCs (**C** and **D**) and Cj-BLCs and Mm-BLCs (**E** and **F**) were tested under the same conditions. All lysates were incubated in the presence or absence of the inhibitors CMK and E64. Data shown are a representative of at least three replicates.

degradation, whereas the Arg46Cit substitution reduced the sensitivity of the Cj-MOG35–51 peptide to degradation. It can also be seen that the CatG inhibitor CMK had less effect than the CatH inhibitor E64 on the proteolytic degradation of the Mm-MOG34–56 Cit^{41} or Mm-MOG34–56 Cit^{46} modifications in the total spleen or $CD20^-$ SC lysate. The two inhibitors were equally effective in the $CD20^+$ SC lysate. Similar effects were observed with the lysate of Cj-SCs (Fig. 8B).

We then tested the degradation of MOG35–51 peptides in lysates of LCV-infected B cells from rhesus monkeys (Mm-BLCs) or marmosets (Cj-BLCs), with or without inhibition of CatG (CMK) or CatH (E64). The results in Fig. 8C show that substitution of the Arg^{46} residue for Cit made the Cj-MOG35–51 peptide resistant to degradation, whereas the Arg^{41} for Cit substitution had no detectable effect. The Arg^{46} for Cit substitution had no effect on the proteolytic degradation of the Mm-MOG35–51 peptide.

In conclusion, the combination of the Arg^{46} to Cit substitution with the presence of a Ser^{42} residue made the complete MOG35–51 peptide resistant against proteolytic degradation in all tested lysates.

Autophagy induction in LCV-infected B cells

Citrullination of antigenic peptides is a physiological process that can take place in autophagosomes of APCs (43). If citrullination of the encephalitogenic MOG34–56 peptide played any role in the conversion of destructive processing to productive processing of the MOG40–48 epitope in LCV-infected B cells, we would expect to observe induction of autophagy and concomitant induction of PAD enzymes by the virus.

In LCV-infected and uninfected cells we analyzed the expression of two PAD genes that are involved in the citrullination of Ag: PAD2 and PAD4. Fig. 9A and 9B show that PAD2 and PAD4, respectively, are highly expressed in Cj-BLCs compared with SCs and fractionated SCs. Interestingly, the PAD2 and PAD4 transcript levels were lower in Mm-BLCs than in Cj-BLCs.

Regarding the relevance of autophagy for cross-presentation by DCs (20), the capacity of the autoantigen to associate with autophagosomes may be a rate-limiting step. The microtubule-associated LC3, and, in particular, the phosphatidylethanolamine-linked isoform LC3-II, is an accepted phagophore/autophagosome marker. LC3-II expressed on the inner membrane of the autophagosomes serves as a docking molecule for cargo binding. We noticed that the Arg^{46} residue is located in a sequence that is a putative LIR motif: [W/Y/F]xx[L/I/V], where x can be any amino acid (21). The motif expressed in the Cj-MOG40–48 epitope is YRSPFSRVV (21).

We reasoned that if autophagy is involved in autoantigen cross-presentation by LCV-infected B cells, infection with the virus should induce the expression of autophagosomes. This was investigated

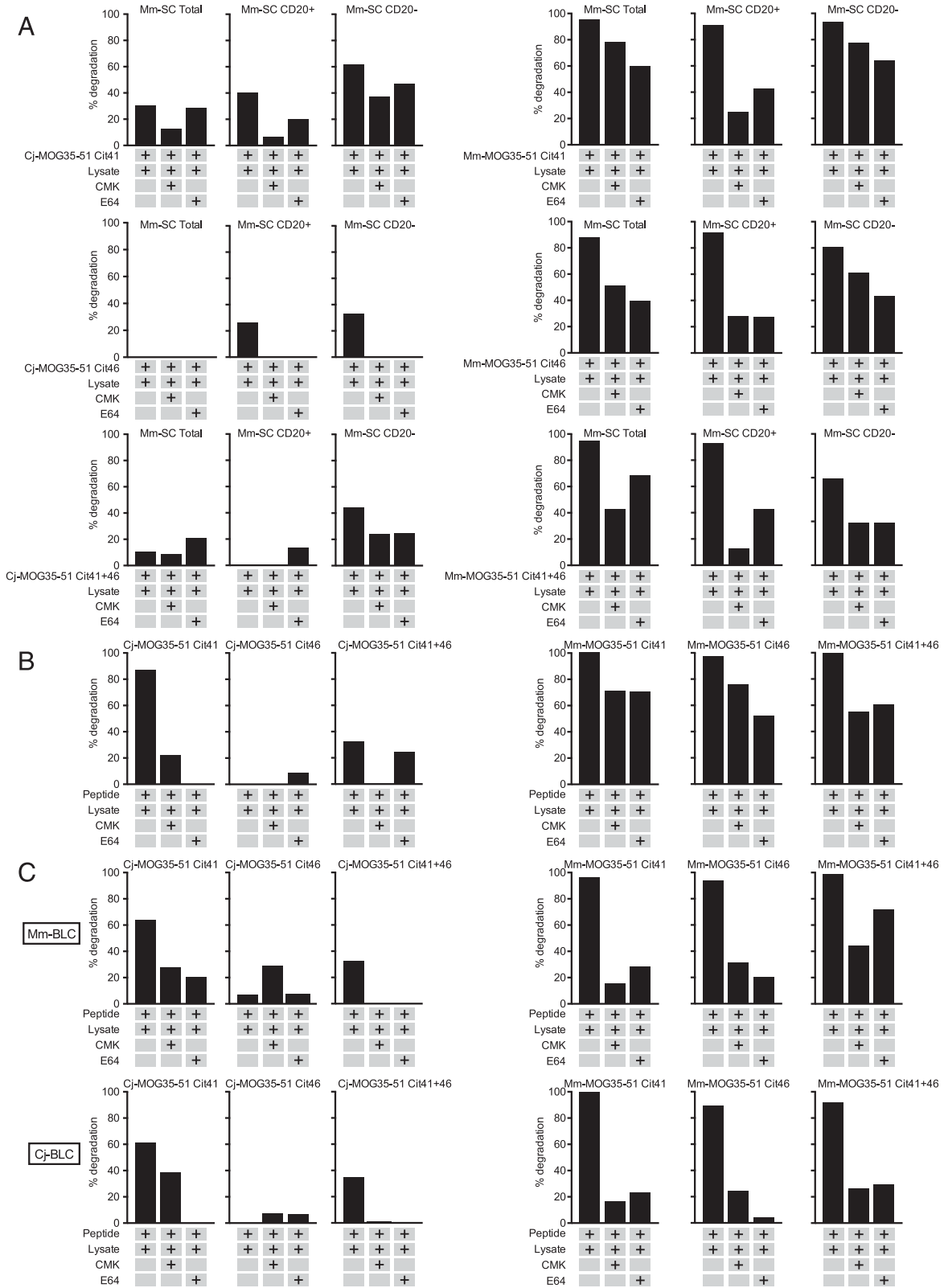

FIGURE 8. Citrullination prevents degradation of MOG peptides. MOG35–51 peptides derived from the marmoset and rhesus monkey sequence were synthesized; Arg at positions 41 and/or 46 were replaced by Cit. The peptides were incubated for 24 h at a fixed concentration (10 μg/ml) with total SC lysate, $CD20^+$ and $CD20^-$ spleen fractions from rhesus monkeys (**A**), marmoset total SCs (**B**), or Mm-BLC lysates and Cj-BLC lysates (**C**). All lysates were incubated in the presence or absence of the inhibitors CMK and E64. The graphs represent the percentage degradation of the indicated peptide. Data shown are a representative of at least three replicates. SDS-PAGE gels are shown in Supplemental Fig. 1.

at the protein and cellular levels. On Western blot, the expression of LC3-I and LC3-II was determined. Fig. 9C and 9D reveal high expression of LC3-II (±14 kDa) in Cj-BLCs. The cell fractions derived from the spleen and Mm-BLCs showed only a marginal expression of LC3-II compared with Cj-BLCs. A similar pattern was observed for LC3-I, although in Mm-BLC, the expression of LC3-I is slightly

higher than LC3-II. The expression of LC3-I was slightly higher than LC3-II in Mm-BLCs. Protein expression of PAD2, PAD4, and LC3 was confirmed on Mm-BLCs and Cj-BLCs with immunofluorescence staining (Fig. 9E). This staining was also performed on total Mm-SCs, $CD20^+$, $CD20^-$, and total Cj-SCs. As expected, these cells were smaller than BLCs and it seemed that relatively fewer $PAD2^+$, $PAD4^+$, and $LC3^+$ cells were observed compared with BLCs.

Discussion

One of the unresolved mysteries in MS is its association with EBV infection (44). Mechanistic studies need to help explain how a virus that infects >90% of the adult human population can be the trigger of a relatively uncommon disease, such as MS, on the appropriate genetic susceptibility background. The observation that EBV is also significantly associated with the risk for systemic lupus erythematosus might suggest that the association is based on generic, in addition to disease-specific, mechanisms. To find an explanation, we used our EAE models in marmosets and rhesus monkeys, nonhuman species that are naturally infected with EBV-related LCV (23).

Collectively, previous data obtained in the marmoset model and replicated in part in rhesus monkeys (reviewed in Refs. 12, 45) show that LCV-infected B cells have a central pathogenic role in the activation of highly pathogenic MHC-E–restricted effector memory cytotoxic T cells that, upon activation with the MOG34–56 peptide (core epitope 40–48), can elicit MS-like pathology and disease. Notably, similar autoaggressive CTLs were found in MS lesions, where they seemed to be engaged in cytotoxic interactions with $HLA\text{-}E^+$ oligodendrocytes (5). The concept that LCV-infected B cells are essential APCs in the immunopathogenic process is supported by the potent clinical effects of depleting anti-CD20 mAbs in MS, which were replicated in the marmoset EAE model (46). These effects are rapid and most likely are not mediated by interference with Ab production, considering that mature plasma cells do not express CD20.

B cells are efficient APCs for $CD4^+$ T cells, because they can capture exogenous Ag at low concentrations via their clonal BCR and then process it in their endolysosomal compartment and present epitopes via MHC class II molecules to $CD4^+$ T cells (16). For presentation of an exogenous Ag via MHC class I molecules to $CD8^+$ T cells, the Ag needs to be translocated from the MHC class II loading compartment to the MHC class I loading compartment. However, B cells seem to be less equipped for presentation of exogenous Ag via MHC class I, a capacity known as Ag cross-presentation (47), at least in the absence of innate immune stimulation (48). Most insight into the mechanisms underlying Ag cross-presentation comes from studies in DCs (17). The $CD8\alpha^+$ mouse DC seems particularly well-equipped for this task (19).

As a basis for our study, we assumed that, analogous to the situation in $CD8\alpha^+$ mouse DCs, LCV infection might endow B cells with cross-presentation capacity when at least two requirements are fulfilled: activation of the cross-presentation machinery and prolongation of the half-life of the CTL epitope.

Activation of the cross-presentation machinery includes immunoproteasome induction for processing of the Ag and induction of costimulatory molecules. The RNA-sequencing data presented in this article show that LCV infection of rhesus monkey B cells induced expression of genes encoding several immunoproteasome elements, supporting the idea that functional immunoproteasomes are formed in LCV-infected B cells. In this study, LCV-infected B cells of rhesus monkeys were well able to induce Ag-specific T cell responses in vivo (18). Hence, we expected to find relevant expression of costimulatory molecules. The RNA-sequencing data show marked mRNA transcript upregulation for CD70 and CD80, whereas mRNAs encoding CD86 and CD40 were reduced. It is of note that CD80 binds preferentially with CTLA4, whereas CD86 is the preferred ligand of CD28 (49). This implies that LCV-infected B cells suppress the activation of naive T cells; however, the constitutively expressed CD70 molecules on mouse DCs relay strong in vivo activation signals to T cells via homodimeric CD27 receptors (50). We reported previously that CD27 is expressed by autoaggressive MOG34–56–specific CTLs induced in the marmoset EAE model (9). Ligand binding to CD27 complements CD28 in determining the size of $CD8^+$ effector memory T cell populations (51). With regard to soluble costimulation factors, we observed that expression of IL-23 mRNA, but not IL-12 mRNA, is highly increased; this is compatible with the observation that autoaggressive CTLs express IL-17A as a signature cytokine (11).

Prolongation of the half-life of the CTL epitope

An important condition for Ag cross-presentation is that fast proteolytic degradation of the Ag in the endolysosomal compartment is suppressed to enable translocation to the MHC class I loading pathway. Indeed, prolongation of the Ag's half-life favors cross-presentation (52). The data presented in this article indicate that, as a consequence of LCV infection, destructive processing of the epitope in B cells is converted into productive processing. To our knowledge, the term "destructive processing" was first coined by Manoury et al. (22) as a mechanism used by thymic APCs to prevent activation of autoreactive T cells.

A key observation is that activation of T cells against the $CD4^+$ T epitope 24–36 is clearly detectable in marmosets immunized with rhMOG/IFA, whereas activation of T cells against the CTL epitope 40–48 was undetectable (10). Nevertheless, the induction of robust encephalitogenic CTL activation in marmosets immunized with MOG34-56/IFA showed that CTLs against the 40–48 epitope are present in the repertoire and can be activated (11). Because a core-pathogenic role for B cells as APCs could be demonstrated in the latter model, we hypothesized that the immunizing MOG34–56 peptide may be rescued from proteolytic degradation when the B cells are infected with the EBV-related LCV CalHV3 (12).

The current study shows that rhMOG is rapidly degraded in cell-free lysates of rhesus monkey and marmoset SCs. Although the strongest proteolytic activity was located in the $CD20^-$ fraction, which contains the myeloid APCs, considerable activity was also found in the $CD20^+$ fraction, which contains the B cells. The activity in BLCs was even lower than in untransformed B cells. Using a protease inhibitor of defined specificity (CMK), we found a dominant role for the serine protease CatG in the proteolytic degradation of rhMOG. Although low transcript levels of CatG mRNA in B cells were measured with qPCR, the enzyme-activity assays show high activity in B cell lysates. Burster et al. (39) reported a similar discrepancy for CatG in the human system. As an explanation, it was proposed that B cells take up exogenous CatG (e.g., produced in myeloid APCs) (53), although this is not a satisfactory explanation for the high CatG activity observed in the LCV-transformed B cell lines. Because CatG is transcribed as proform, the activity could be due to variations in activation and deactivation of the bioactive enzyme (54). We also observed inhibition of rhMOG degradation by the cysteine protease inhibitor E64. It is unclear whether this effect can be attributed to the inhibition of CatH, because E64 is a general cysteine protease inhibitor that also inhibits CatC, which is the activator of serine cathepsins, including CatG. The two inhibitors were strongly effective in lysates of rhesus monkey SCs but were only moderately effective in lysates of marmoset SCs. Both inhibitors were also fully effective in the $CD20^+$ B cell fraction of rhesus monkey SCs. The observed species differences might be attributed, in part, to the specificity difference of CatG from marmosets and

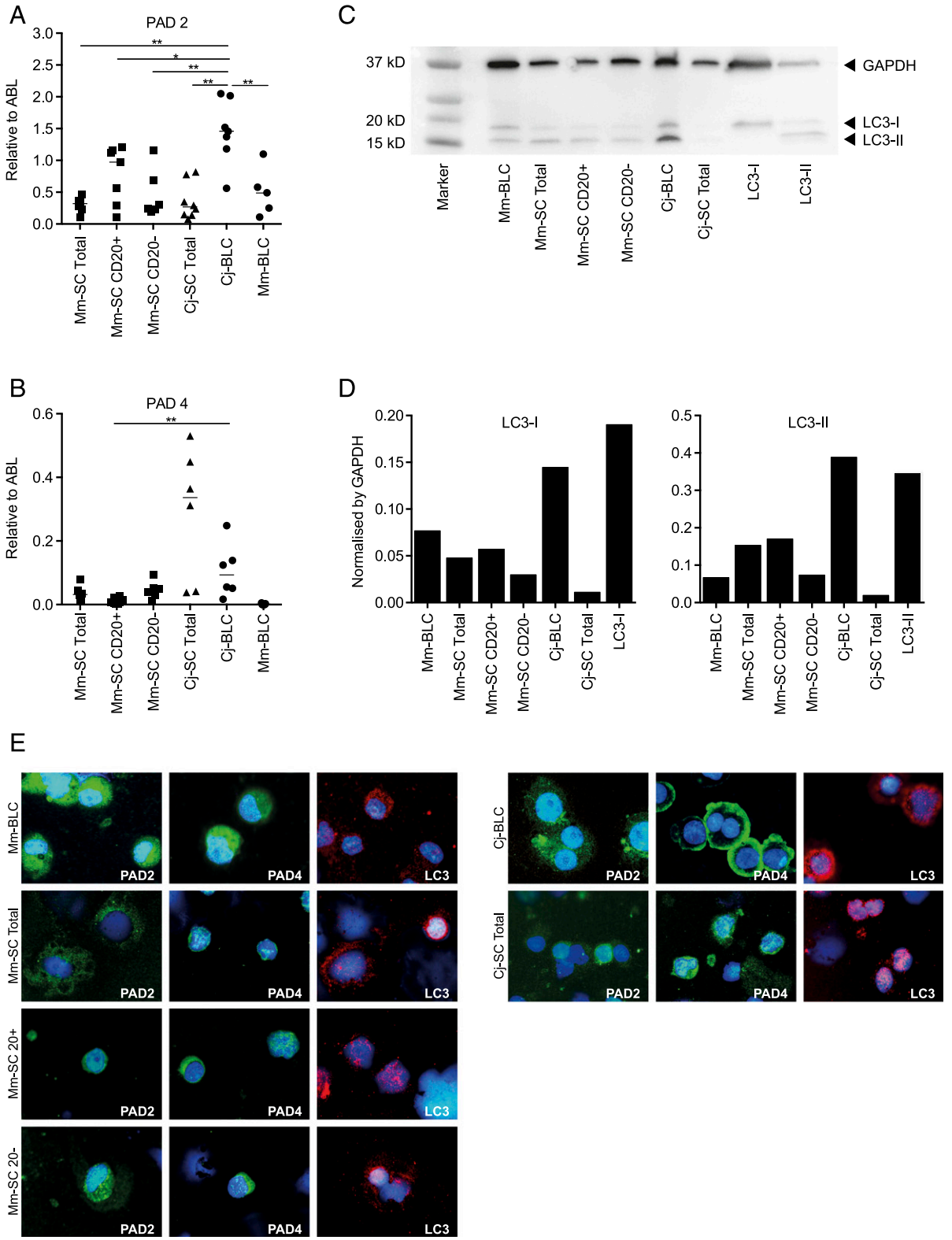

FIGURE 9. Expression of PAD and LC3 in LCV-infected B cells. Total RNA was extracted from different cell lysates to determine expression of mRNA encoding PAD2 (**A**) and PAD4 (**B**) by qPCR. Transcript levels were normalized against the reference gene ABL. Median of each cell population is shown. (**C**) Cell lysates were immune-blotted for LC3 and GAPDH as loading control. As positive controls, Abs against LC3-I and LC3-II were run along with the other samples. (**D**) The density of the LC3-I and LC3-II band in (C) is related to the GAPDH band. (**E**) Immunofluorescence staining was performed with rhesus monkey cells (left panel) and marmoset cells (right panel) with anti-PAD2, anti-PAD4, and anti-LC3. Original magnification ×400. $*p < 0.05$, $**p < 0.001$, Cj-BLC/Mm-BLC versus other cell subsets, Mann–Whitney *U* test.

rhesus monkeys. Although CatG of marmosets has a mouse-like narrow specificity for aromatic (chymotryptic) cleavage sites (Trp, Phe, Tyr), a double mutation in the specificity-determining residues (Ala-189-Ser and Glu-226-Ala) broadens the activity of rhesus monkey and human CatG to basic (tryptic) cleavage sites (e.g., Arg and Lys) (42).

To test the proteolytic degradation of the pathogenically dominant Mm-MOG34-56 peptide we used the shorter peptide MOG35-51 to avoid interference of the Arg residue at position 52, which is outside the epitope of interest (residues 40–48). The reported in vitro data show that native Mm-MOG35-51 peptide is rapidly degraded in cell-free lysates of noninfected and LCV infected B cells of rhesus monkeys as well as in LCV-infected B cells of marmosets. Again, a dominant role of the endolysosomal protease CatG in the degradation of Mm-MOG35-51 was observed. Interestingly, substitution of the Pro^{42} residue for Ser and the Arg46 residues for Cit conferred complete resistance of the MOG35-51 peptide to proteolytic degradation in the rhesus monkey cell lysates. Substitution of the Arg41 residue for Cit had no detectable effect. How can this be explained?

The alignment of MOG extracellular domain sequences (Fig. 5) shows that, in a wide range of mammalian species, a Pro residue is present at position 42, whereas a Ser is present at this position only in rat, mouse, and marmoset MOG. Data obtained from mice show that the presence of a Pro or Ser residue on position 42 has a strong influence on the encephalitogenic potency of the MOG34–56 peptide (55). The Arg to Cit substitution is a physiologically relevant modification of antigenic peptides, mediated by the enzyme PAD (43), which can occur in stressed B cells, such as those infected by LCV. The investigators claim that citrullination by PAD occurs in autophagosomes. It is well-documented that LCV infection of B cells induces autophagy (56). Consistent with this notion, our RNA-sequencing data showed increased expression of autophagy-related genes, such as beclin1, ATG5, and ATG12, in LCV-infected B cells of rhesus monkeys. Moreover, we show that the autophagosome marker LC3-II is increased in LCV-infected B cells of rhesus monkeys.

Autophagosomes are implicated in cross-presentation (20). On the basis of the data presented in this article, we propose that they are also engaged in the protection of MOG peptide against destructive processing. We assumed that, for association of the MOG35–51 peptide with LC3 molecules in the inner concave surface of growing autophagosomes, the peptide should contain a LIR motif. The consensus sequence of LIR motifs is [W/Y/F]xx[L/I/V], where x can be any amino acid (21). In addition to this core motif, the presence of an acidic residue (E, D, S, T) close to the N-terminal site of the LIR motif is important. Using this algorithm, we scanned the rhMOG sequences of marmoset and rhesus monkeys and found three potential LIR motifs: residues 3–6 (FRVI), 44–47 (FSRV), and 118–122 (FYWV). The $^{44}FSRV^{47}$ LIR motif is encompassed within the pathogenically relevant MOG40–48 epitope. In the marmoset MOG sequence, it is preceded by Ser^{42}, which contains the favorable Ser^{42} residue for LC3 association. Because the CatG cleavage site Arg^{46} is inside the LIR motif, we speculate that substitution of the Arg^{46} residue for Cit prevents cleavage of the LIR motif by CatG.

In conclusion, based on the results of this study we propose a physiological role for B cells in the protection against autoimmunity in MS. They take up autoantigens and neutralize them via destructive processing; in this way, activation of autoaggressive $CD8^+$ T cells is avoided. By infection of B cells with LCV, this protective mechanism is converted into productive processing of the autoantigen, which enables the activation of autoaggressive T cells. The proposed underlying mechanism is that, as a result of several cell-biological changes induced in the B cells, in particular the formation of autophagosomes with which the encephalitogenic Ag may associate, the $CD8^+$ T cell epitope is protected against degradation and remains available for cross-presentation.

Acknowledgments

We thank Nieske Brouwer (Department of Neuroscience, UMCG) and Pieter van der Vlies (Department of Genetics, UMCG) for technical assistance with RNA sequencing, Francisca van Hassel for artwork, and Prof. Fulvio Reggiori (Department of Cell Biology, UMCG) for expert advice on autophagy.

Disclosures

The authors have no financial conflicts of interest.

References

1. Gold, R., C. Linington, and H. Lassmann. 2006. Understanding pathogenesis and therapy of multiple sclerosis via animal models: 70 years of merits and culprits in experimental autoimmune encephalomyelitis research. *Brain* 129: 1953–1971.
2. Wekerle, H., and F. C. Kurschus. 2006. Animal models of multiple sclerosis. *Drug Discov. Today Dis. Models* 3: 359–367.
3. Simmons, S. B., E. R. Pierson, S. Y. Lee, and J. M. Goverman. 2013. Modeling the heterogeneity of multiple sclerosis in animals. *Trends Immunol.* 34: 410–422.
4. 't Hart, B. A., B. Gran, and R. Weissert. 2011. EAE: imperfect but useful models of multiple sclerosis. *Trends Mol. Med.* 17: 119–125.
5. Zaguia, F., P. Saikali, S. Ludwin, J. Newcombe, D. Beauseigle, E. McCrea, P. Duquette, A. Prat, J. P. Antel, and N. Arbour. 2013. Cytotoxic NKG2C+ CD4 T cells target oligodendrocytes in multiple sclerosis. *J. Immunol.* 190: 2510–2518.
6. Jagessar, S. A., P. A. Smith, E. Blezer, C. Delarasse, D. Pham-Dinh, J. D. Laman, J. Bauer, S. Amor, and B. 't Hart. 2008. Autoimmunity against myelin oligodendrocyte glycoprotein is dispensable for the initiation although essential for the progression of chronic encephalomyelitis in common marmosets. *J. Neuropathol. Exp. Neurol.* 67: 326–340.
7. Brok, H. P., A. Uccelli, N. Kerlero De Rosbo, R. E. Bontrop, L. Roccatagliata, N. G. de Groot, E. Capello, J. D. Laman, K. Nicolay, G. L. Mancardi, et al. 2000. Myelin/oligodendrocyte glycoprotein-induced autoimmune encephalomyelitis in common marmosets: the encephalitogenic T cell epitope pMOG24-36 is presented by a monomorphic MHC class II molecule. *J. Immunol.* 165: 1093–1101.
8. Kap, Y. S., P. Smith, S. A. Jagessar, E. Remarque, E. Blezer, G. J. Strijkers, J. D. Laman, R. Q. Hintzen, J. Bauer, H. P. Brok, and B. A. 't Hart. 2008. Fast progression of recombinant human myelin/oligodendrocyte glycoprotein (MOG)-induced experimental autoimmune encephalomyelitis in marmosets is associated with the activation of MOG34-56-specific cytotoxic T cells. *J. Immunol.* 180: 1326–1337.
9. Jagessar, S. A., N. Heijmans, E. L. Blezer, J. Bauer, J. H. Blokhuis, J. A. Wubben, J. W. Drijfhout, P. J. van den Elsen, J. D. Laman, and B. A. 't Hart. 2012. Unravelling the T-cell-mediated autoimmune attack on CNS myelin in a new primate EAE model induced with MOG34-56 peptide in incomplete adjuvant. *Eur. J. Immunol.* 42: 217–227.
10. Jagessar, S. A., N. Heijmans, E. L. Blezer, J. Bauer, R. Weissert, and B. A. 't Hart. 2015. Immune profile of an atypical EAE model in marmoset monkeys immunized with recombinant human myelin oligodendrocyte glycoprotein in incomplete Freund's adjuvant. *J. Neuroinflammation* 12: 169.
11. Jagessar, S. A., Y. S. Kap, N. Heijmans, N. van Driel, L. van Straalen, J. J. Bajramovic, H. P. Brok, E. L. Blezer, J. Bauer, J. D. Laman, and B. A. 't Hart. 2010. Induction of progressive demyelinating autoimmune encephalomyelitis in common marmoset monkeys using MOG34-56 peptide in incomplete freund adjuvant. *J. Neuropathol. Exp. Neurol.* 69: 372–385.
12. 't Hart, B. A., S. A. Jagessar, K. Haanstra, E. Verschoor, J. D. Laman, and Y. S. Kap. 2013. The primate EAE model points at EBV-infected B cells as a preferential therapy target in multiple sclerosis. *Front. Immunol.* 4: 145.
13. Jagessar, S. A., N. Heijmans, L. Oh, J. Bauer, E. L. Blezer, J. D. Laman, T. S. Migone, M. N. Devalaraja, and B. A. 't Hart. 2012. Antibodies against human BLyS and APRIL attenuate EAE development in marmoset monkeys. *J. Neuroimmune Pharmacol.* 7: 557–570.
14. Kap, Y. S., N. van Driel, E. Blezer, P. W. Parren, W. K. Bleeker, J. D. Laman, J. L. Craigen, and B. A. 't Hart. 2010. Late B cell depletion with a human anti-human CD20 IgG1κ monoclonal antibody halts the development of experimental autoimmune encephalomyelitis in marmosets. *J. Immunol.* 185: 3990–4003.
15. Anwar Jagessar, S., Z. Fagrouch, N. Heijmans, J. Bauer, J. D. Laman, L. Oh, T. Migone, E. J. Verschoor, and B. A. 't Hart. 2013. The different clinical effects of anti-BLyS, anti-APRIL and anti-CD20 antibodies point at a critical pathogenic role of γ-herpesvirus infected B cells in the marmoset EAE model. *J. Neuroimmune Pharmacol.* 8: 727–738.
16. Avalos, A. M., and H. L. Ploegh. 2014. Early BCR events and antigen capture, processing, and loading on MHC class II on B cells. *Front. Immunol.* 5: 92.
17. Joffre, O. P., E. Segura, A. Savina, and S. Amigorena. 2012. Cross-presentation by dendritic cells. *Nat. Rev. Immunol.* 12: 557–569.
18. Haanstra, K. G., J. A. Wubben, M. Jonker, and B. A. 't Hart. 2013. Induction of encephalitis in rhesus monkeys infused with lymphocryptovirus-infected B-cells presenting MOG(34–56) peptide. *PLoS One* 8: e71549.
19. Dudziak, D., A. O. Kamphorst, G. F. Heidkamp, V. R. Buchholz, C. Trumpfheller, S. Yamazaki, C. Cheong, K. Liu, H. W. Lee, C. G. Park, et al. 2007. Differential antigen processing by dendritic cell subsets in vivo. *Science* 315: 107–111.
20. Mintern, J. D., C. Macri, W. J. Chin, S. E. Panozza, E. Segura, N. L. Patterson, P. Zeller, D. Bourges, S. Bedoui, P. J. McMillan, et al. 2015. Differential use of autophagy by primary dendritic cells specialized in cross-presentation. *Autophagy* 11: 906–917.
21. Birgisdottir, A. B., T. Lamark, and T. Johansen. 2013. The LIR motif - crucial for selective autophagy. *J. Cell Sci.* 126: 3237–3247.

22. Manoury, B., D. Mazzeo, L. Fugger, N. Viner, M. Ponsford, H. Streeter, G. Mazza, D. C. Wraith, and C. Watts. 2002. Destructive processing by asparagine endopeptidase limits presentation of a dominant T cell epitope in MBP. *Nat. Immunol.* 3: 169–174.
23. Gerner, C. S., A. Dolan, and D. J. McGeoch. 2004. Phylogenetic relationships in the Lymphocryptovirus genus of the Gammaherpesvirinae. *Virus Res.* 99: 187–192.
24. Jagessar, S. A., M. Vierboom, E. L. Blezer, J. Bauer, B. A. 't Hart, and Y. S. Kap. 2013. Overview of models, methods, and reagents developed for translational autoimmunity research in the common marmoset (*Callithrix jacchus*). *Exp. Anim.* 62: 159–171.
25. Andrews, S. 2014. FastQC, a quality control tool for high throughput Sequence data, version 0.11.3. Babraham Institute, Cambridge, U. K. http://www.bioinformatics.babraham.ac.uk/projects/fastqc/.
26. Kim, D., G. Pertea, C. Trapnell, H. Pimentel, R. Kelley, and S. L. Salzberg. 2013. TopHat2: accurate alignment of transcriptomes in the presence of insertions, deletions and gene fusions. *Genome Biol.* 14: R36.
27. Anders, S., P. T. Pyl, and W. Huber. 2015. HTSeq–a Python framework to work with high-throughput sequencing data. *Bioinformatics* 31: 166–169.
28. Robinson, M. D., D. J. McCarthy, and G. K. Smyth. 2010. edgeR: a Bioconductor package for differential expression analysis of digital gene expression data. *Bioinformatics* 26: 139–140.
29. Durinck, S., P. T. Spellman, E. Birney, and W. Huber. 2009. Mapping identifiers for the integration of genomic datasets with the R/Bioconductor package biomaRt. *Nat. Protoc.* 4: 1184–1191.
30. Smith, P. A., N. Heijmans, B. Ouwerling, E. C. Breij, N. Evans, J. M. van Noort, A. C. Plomp, C. Delarasse, B. 't Hart, D. Pham-Dinh, and S. Amor. 2005. Native myelin oligodendrocyte glycoprotein promotes severe chronic neurological disease and demyelination in Biozzi ABH mice. *Eur. J. Immunol.* 35: 1311–1319.
31. van Kasteren, S. I., I. Berlin, J. D. Colbert, D. Keane, H. Ovaa, and C. Watts. 2011. A multifunctional protease inhibitor to regulate endolysosomal function. *ACS Chem. Biol.* 6: 1198–1204.
32. Rose, N. L., M. M. Palcic, L. M. Helms, and J. R. Lakey. 2003. Evaluation of Pefabloc as a serine protease inhibitor during human-islet isolation. *Transplantation* 75: 462–466.
33. Lomas, D. A., S. R. Stone, C. Llewellyn-Jones, M. T. Keogan, Z. M. Wang, H. Rubin, R. W. Carrell, and R. A. Stockley. 1995. The control of neutrophil chemotaxis by inhibitors of cathepsin G and chymotrypsin. *J. Biol. Chem.* 270: 23437–23443.
34. Barrett, A. J., A. A. Kembhavi, M. A. Brown, H. Kirschke, C. G. Knight, M. Tamai, and K. Hanada. 1982. L-trans-Epoxysuccinyl-leucylamido (4-guanidino)butane (E-64) and its analogues as inhibitors of cysteine proteinases including cathepsins B, H and L. *Biochem. J.* 201: 189–198.
35. Méthot, N., J. Rubin, D. Guay, C. Beaulieu, D. Ethier, T. J. Reddy, D. Riendeau, and M. D. Percival. 2007. Inhibition of the activation of multiple serine proteases with a cathepsin C inhibitor requires sustained exposure to prevent pro-enzyme processing. *J. Biol. Chem.* 282: 20836–20846.
36. Steimle, V., C. A. Siegrist, A. Mottet, B. Lisowska-Grospierre, and B. Mach. 1994. Regulation of MHC class II expression by interferon-gamma mediated by the transactivator gene CIITA. *Science* 265: 106–109.
37. Kobayashi, K. S., and P. J. van den Elsen. 2012. NLRC5: a key regulator of MHC class I-dependent immune responses. *Nat. Rev. Immunol.* 12: 813–820.
38. Blum, J. S., P. A. Wearsch, and P. Cresswell. 2013. Pathways of antigen processing. *Annu. Rev. Immunol.* 31: 443–473.
39. Burster, T., A. Beck, E. Tolosa, V. Marin-Esteban, O. Rötzschke, K. Falk, A. Lautwein, M. Reich, J. Brandenburg, G. Schwarz, et al. 2004. Cathepsin G, and not the asparagine-specific endoprotease, controls the processing of myelin basic protein in lysosomes from human B lymphocytes. *J. Immunol.* 172: 5495–5503.
40. Dodt, J., and J. Reichwein. 2003. Human cathepsin H: deletion of the mini-chain switches substrate specificity from aminopeptidase to endopeptidase. *Biol. Chem.* 384: 1327–1332.
41. Rothe, M., and J. Dodt. 1992. Studies on the aminopeptidase activity of rat cathepsin H. *Eur. J. Biochem.* 210: 759–764.
42. Raymond, W. W., N. N. Trivedi, A. Makarova, M. Ray, C. S. Craik, and G. H. Caughey. 2010. How immune peptidases change specificity: cathepsin G gained tryptic function but lost efficiency during primate evolution. *J. Immunol.* 185: 5360–5368.
43. Ireland, J. M., and E. R. Unanue. 2012. Processing of proteins in autophagy vesicles of antigen-presenting cells generates citrullinated peptides recognized by the immune system. *Autophagy* 8: 429–430.
44. Ascherio, A., K. L. Munger, and J. D. Lünemann. 2012. The initiation and prevention of multiple sclerosis. *Nat. Rev. Neurol.* 8: 602–612.
45. 't Hart, B. A., Y. van Kooyk, J. J. Geurts, and B. Gran. 2015. The primate autoimmune encephalomyelitis model; a bridge between mouse and man. *Ann. Clin. Transl. Neurol.* 2: 581–593.
46. Jagessar, S. A., N. Heijmans, J. Bauer, E. L. Blezer, J. D. Laman, N. Hellings, and B. A. 't Hart. 2012. B-cell depletion abrogates T cell-mediated demyelination in an antibody-nondependent common marmoset experimental autoimmune encephalomyelitis model. *J. Neuropathol. Exp. Neurol.* 71: 716–728.
47. Cresswell, P., A. L. Ackerman, A. Giodini, D. R. Peaper, and P. A. Wearsch. 2005. Mechanisms of MHC class I-restricted antigen processing and cross-presentation. *Immunol. Rev.* 207: 145–157.
48. Jiang, W., M. M. Lederman, C. V. Harding, and S. F. Sieg. 2011. Presentation of soluble antigens to CD8+ T cells by CpG oligodeoxynucleotide-primed human naive B cells. *J. Immunol.* 186: 2080–2086.
49. Pentcheva-Hoang, T., J. G. Egen, K. Wojnoonski, and J. P. Allison. 2004. B7-1 and B7-2 selectively recruit CTLA-4 and CD28 to the immunological synapse. *Immunity* 21: 401–413.
50. Keller, A. M., A. Schildknecht, Y. Xiao, M. van den Broek, and J. Borst. 2008. Expression of costimulatory ligand CD70 on steady-state dendritic cells breaks CD8+ T cell tolerance and permits effective immunity. *Immunity* 29: 934–946.
51. Yamada, A., A. D. Salama, M. Sho, N. Najafian, T. Ito, J. P. Forman, R. Kewalramani, S. Sandner, H. Harada, M. R. Clarkson, et al. 2005. CD70 signaling is critical for CD28-independent CD8+ T cell-mediated alloimmune responses in vivo. *J. Immunol.* 174: 1357–1364.
52. Delamarre, L., R. Couture, I. Mellman, and E. S. Trombetta. 2006. Enhancing immunogenicity by limiting susceptibility to lysosomal proteolysis. *J. Exp. Med.* 203: 2049–2055.
53. Burster, T., H. Macmillan, T. Hou, B. O. Boehm, and E. D. Mellins. 2010. Cathepsin G: roles in antigen presentation and beyond. *Mol. Immunol.* 47: 658–665.
54. van Kasteren, S. I., and H. S. Overkleeft. 2014. Endo-lysosomal proteases in antigen presentation. *Curr. Opin. Chem. Biol.* 23: 8–15.
55. Oliver, A. R., G. M. Lyon, and N. H. Ruddle. 2003. Rat and human myelin oligodendrocyte glycoproteins induce experimental autoimmune encephalomyelitis by different mechanisms in C57BL/6 mice. *J. Immunol.* 171: 462–468.
56. Lee, D. Y., and B. Sugden. 2008. The latent membrane protein 1 oncogene modifies B-cell physiology by regulating autophagy. *Oncogene* 27: 2833–2842.